Experimental Investigation of Dimples as a Heat Transfer Enhancement Feature in Narrow Diverging and Converging Channels

Shreyas Srinivasan

Thesis submitted to the faculty of the Virginia Polytechnic Institute and State University in partial fulfillment of the requirements for the degree of

Master of Science
In
Mechanical Engineering

Srinath V. Ekkad, Chair.
Danesh K. Tafti
Lin Ma

July 12th, 2013
Blacksburg VA

Keywords: Heat transfer, Narrow channels, Dimples, Heat transfer enhancements.

Experimental Investigation of Dimples as a Heat Transfer Enhancement Feature in Narrow Diverging and Converging Channels

Shreyas Srinivasan

ABSTRACT

Detailed heat transfer coefficient distributions have been obtained for narrow converging and diverging channels with and without enhancement features. The enhancement feature considered for this study is dimples (inline and staggered) on the main heat transfer surfaces. All the measurements are presented at Reynolds numbers of 3500, 8900, 18000, and 7000, 14000, 28000 for converging and diverging channels respectively. Pressure drop measurements for the overall channel are also presented to evaluate the heat transfer enhancement geometry with respect to pumping power requirements. The test models were studied for wall heat transfer coefficient measurements using the transient liquid crystal technique. The modeled wall inner surfaces were sprayed with thermochromic liquid crystals, and a transient test was used to obtain the local heat transfer coefficients from the measured color change. Analysis of results shows that dimples, in general, have very good enhancement capabilities and staggered dimpled surfaces provide considerably higher heat transfer coefficients and a reasonable pressure drop compared to inline dimpled configuration.

Additionally, this study was extended to understand the effect of strategic placement of dimples (staggered) at various locations along the channel to understand regions that contribute significantly to the overall enhancement.

Acknowledgements

It is because of Amma, Nana, and Shrikanth, I have succeeded this far in life. I would not have been here without you. Your unconditional love, encouragement, and support have shaped me to be the man I am today. I must thank and appreciate my fiancée, Sahana, for her patience, undivided attention, understanding, and ever available shoulder to have tolerated me through all of my phases. Any amount of thanks to her would be little.

I sincerely thank Dr. Srinath V. Ekkad to have supported and guided me through this entire eventful journey. I am ever indebted to him for lighting my path with motivation and supervision. I am very grateful to him for being my academic advisor and most importantly, for being my Guru. He is one of the strongest influences on me to help me realize my potential.

I thank Anil Tolpadi and many others at GE Energy that I have worked with. Interactions with you have always left me with a strong and positive impression.

Importantly, I would like to thank all my friends, particularly, Justin Lamont, Bonaventure R. Nunes, Vivek Kumar, David Gomez Ramirez, Grant Jiang, Deepu Dilip and many others for helping me with research, coursework, and on the whole, making my graduate school experience very enjoyable.

Thanks to my roommates, Sriram and Naresh who threw some light for me on cooking, and helped me synchronize with the fast-paced graduate life. I thank you both for the nice memories and lifelong friendships.

Lastly, but in contrast, most importantly, I would like to thank Lord Ganesh to have been an important and integral part of my journey through life by showering his divine blessings from time to time.

Table of Contents

Table of Figures

Table of tables

1 Introduction

Heat exchange process has proven to be ubiquitous in today's world. Every industrial, commercial and domestic application's conversion, utilization and recovery involves a process of heat exchange. There are ample instances not limited to steam generation plants, thermal processing of chemical and agricultural products resulting in heating and cooling of viscous media, refrigeration evaporation, fluid cooling of turbomachinery and auto engine systems, cooling of electrical equipment, electronic devices, etc. which welcome improved heat exchange. This can directly translate into improving the thermal efficiency of the process in addition to the economics of their design and operation.

The emergence of heat transfer enhancement is mainly due to the need to increase the thermal performance of machines, thereby to produce an effect in saving of energy, material, and costs additionally resulting in a natural reduction of environmental degradation. When designing cooling systems for automobiles and spacecraft, it is imperative that the heat exchangers are especially compact and lightweight. Enhancement techniques essentially reduce the thermal resistance by promoting higher convective heat transfer with or without an increase in surface area.

1.1 Convective Heat Transfer

Convective heat transfer is the transport mechanism made possible through the motion of fluid. Natural and forced convection are the two types of convection. The type of convective heat transfer that will be dealt throughout this study is the forced type, where a fluid is forced to flow over a surface or inside a channel by the means of external source such as pumps, fans, etc. The controlling equation for convection is given by Newton's law of cooling in cases where the heat transfer coefficient is independent of the temperature difference between object and environment. Isaac Newton modeled the cooling process by assuming that the rate at which thermal energy displaced from one body to another is proportional to the temperature difference between them.

$$\frac{dQ}{dt} = hA\left(T_{obj} - T_{env}\right) \tag{1.1}$$

Where, Q is the thermal energy in Joules, A is the total convective area, h being the convective heat transfer coefficient in W/m^2K, T_{obj} and T_{env} are the temperatures of the object and environment in K respectively.

The heat transfer coefficient defines the ease with which heat passes from the fluid to the environment or vice versa. Heat will always flow from hot to cold for materials in direct contact. Heat transfer coefficient is considered when designing equipment that is specifically intended to transfer heat or to not transfer heat. There

exist various factors that can impact the convective heat transfer coefficient. Geometry (flat plate, cylinder, size, aspect ratio, vertical or horizontal placement), type of flow (forced, natural, laminar, turbulent, developing, fully developed, etc.), type of fluid and its properties play a significant role in convective heat transfer.

1.2 Parameter Introduction – Reynolds Number (Re)

A parameter that plays an important role in this study as well as in fluid dynamics is a dimensionless number that gives the ratio of inertial forces to viscous forces called the Reynolds number (Re). It is used to characterize flow regimes to be laminar or turbulent. Laminar flows occur at low Re where viscous forces dominate over inertial forces. While turbulent flows occur at high Re where inertial forces dominate producing eddies, vortices and other flow instabilities. For flow in a channel, the Reynolds number is given by,

$$Re = \frac{\rho v D_H}{\mu} \tag{1.2}$$

Where ρ is the density of the fluid in kg/m^3, v is the velocity in m/s, D_H is the hydraulic diameter in m and μ being the dynamic viscosity of the fluid in $kg/(m.s)$. For shapes like squares, rectangular or any quadrilateral, the dimension for internal flow situations is given by the hydraulic diameter given as.

$$D_H = \frac{4A}{P} \tag{1.3}$$

Where A is the area of the cross-sectional area of the channel while P forms the perimeter.

1.3 Importance of Cooling in Power Generation Industry

For gas turbines, cooling channels are used in the turbine section where hot gases greatly exceed the material melting point. The compressor of a gas turbine sucks in air, compresses it, mixes and ignites with fuel in the combustion chamber and the hot gases expand through the turbine section where the energy is mined. The trend in the gas turbine industry is to reach higher ignition temperatures which would produce more complete combustion and therefore increasing the efficiency and performance of the engines. The hot gas path components need to be actively cooled during operation to prevent failure due to high thermal stresses. Since the blade and vane components are hollow to an extent, coolant channels are constructed to dissipate heat maintaining the structural integrity of the components. One of the sources for coolant is tapped from the compressor which takes approximately 5% of compressed air which is at 500°C and Reynolds number ranging in the excess of 25,000 and 100,000 for aircraft and land based turbines respectively. Hence, if this requirement for compressed air is substituted, performance will be increased.

In this thesis, a general study of heat transfer characteristics is made in low aspect ratio converging and diverging channels which finds plethora of applications in gas turbines, + channels in industrial electricity generators, steam turbines, electronic and electric components, etc. Figure 1.1 and 1.2 show the cooling configuration for stator coil of industrial electric generators where such channels could find relevance.

The research involved with this study is purely experimental, therefore a transient liquid crystal technique is implemented that determines heat transfer coefficient, h, inside the coolant channels.

This thesis focuses on the effects of heat transfer in presence of a heat transfer enhancement feature called dimples in narrow converging and diverging channels. As a part of this study, two types of dimple configurations are investigated – inline and stagger type. By extension, heat transfer in a smooth wall is studied to develop a baseline understanding of the narrow channels.

Experimental investigations of such coolant channels will benefit Computational Fluid Dynamics modeling. Understanding the physics of the flows, engineers will have access to more information and tools to optimize the coolant channel designs to attain more outcome, reducing the usage of coolant and try to extend a machine's operational life.

The main objective of this study is to develop an experimental set up that can model coolant channels under stable stationary conditions.

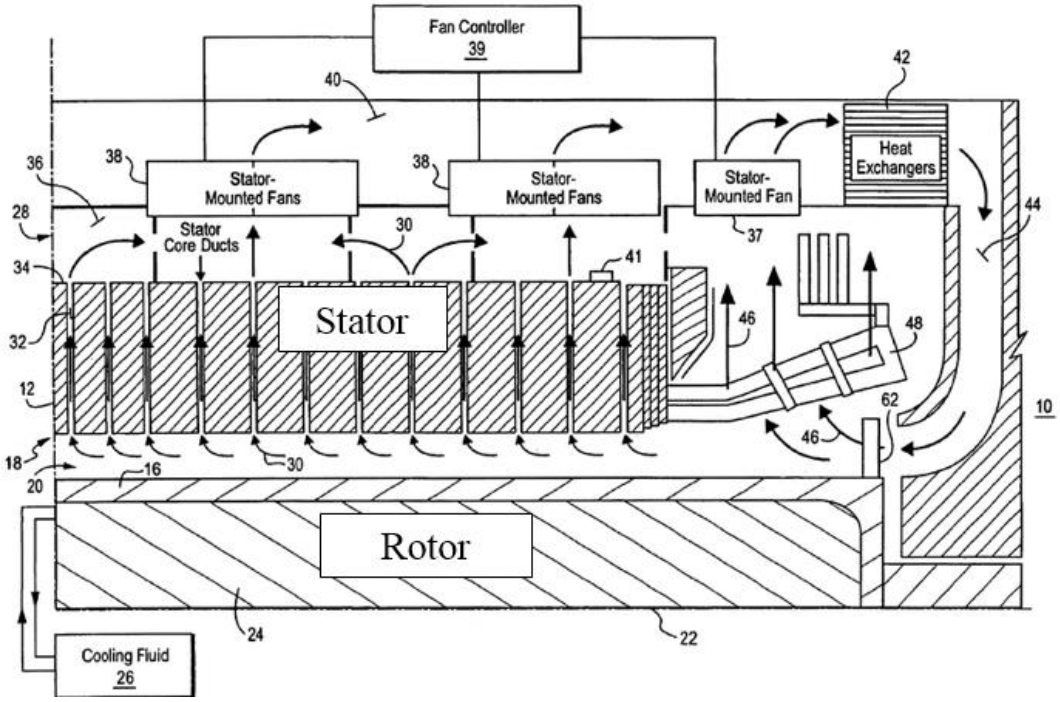

Figure 1.1: Schematic of an electric generator. Courtesy: GE Company (© FPO, United States Patent - 6882068)

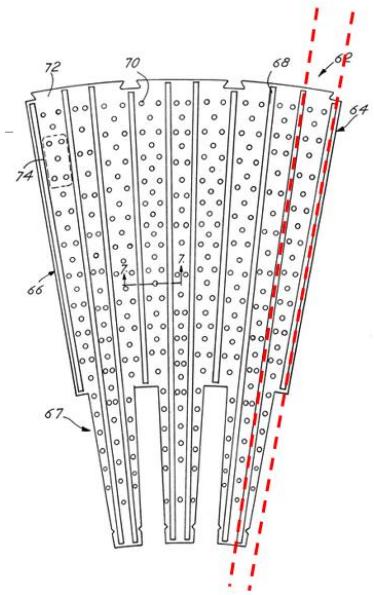

Figure 1.2: Stator coolant channels

2 Literature Survey

2.1 Introduction

Early studies are introduced in the field of internal flows to lay a foundation of understanding in the fluid physics. The physics are extremely important which holds an ultimate control over heat transfer distributions. These studies are introduced to develop a baseline validation for the research that ensues. Cooling techniques are classified into active and passive cooling techniques. This study focuses only on a passive cooling technique to provide turbulation, called dimples. Although, many studies have addressed enhancement features such as ribs, protrusions, jet impingement, etc. A wide range of coolant geometries are in place today, which are explored to match the requirement and extract the maximum amount of benefit possible. This research is aimed at understanding of heat transfer in low aspect ratio channels with converging and diverging profiles. To understand why the topic heads in this direction, current state of art in cooling narrow channels is discussed.

2.2 Earlier Studies

Dimples are a very attractive feature of increasing internal cooling since they trigger the formation of multiple vortex pairs that produce significant enhancement in heat transfer coefficient as the flow passes over it. The advent of dimple or in a

more nascent form called the hemispherical indentation was brought to light through aerodynamics. In 1966, Snedeker & Donaldson performed an experimental study of the flow induced inside a transparent full hemispherical cavity fastened to the floor of the test section of a wind tunnel. A movable tuft was being used by the authors to observe the flow patterns due to the cavity. A steady vortex was constantly observed irrespective of the velocity skewed at an angle to the mainstream direction.

Keeping this in perspective, usage of dimples for heat transfer augmentation were explored to a deep level in the late Union of Soviet Socialist Republics. Sometime around 1986, Murzin et al. performed an experimental study to understand and characterize the flow behavior posed by a hemispherical indentation in the channel wall. Based on the study, the authors conclude that the flow is mostly symmetric and consist of recirculatory zones in the depression. This particular characteristic of the flow by the feature proved to be the major contributor towards heat transfer enhancement. Murzin et al.'s observations were further proved by Gromov et al. They contributed detailed results supporting the observation of stable, symmetric recirculatory zones or vortex structures. Kesarev and Kozlov investigated local heat transfer coefficients on the surface of a hemispherical cavity finding that the position of streamlines along the cavity indicate a vortex formation. It is also

found out that the mean heat transfer coefficient on the cavity is increased as the free stream turbulence level grows.

At Moscow State Technical University, in 1993, Afanasyev et al. conducted experiments to measure heat transfer and friction factors with spherical cavities with turbulent flow. The authors observe a heat transfer enhancement of about 30-40% without much increase in pressure loss. They mention that the main reasons for this enhancement is due to the deterioration of thickness of the viscous sublayer and promotion of recirculatory or vortex flow structures caused by the spherical indentation.

Laser diagnostics had marked its beginning in the many research areas, including heat transfer and fluid physics. Terekhov et al. were among the first to provide quantitative measurements of flow physics underlying the dimple geometry using laser diagnostics. Results showed that auto-oscillations of the flow arise from the dimpled surface for all of the experimental conditions tested, with a single monovortex structure switching between two positions. The authors also performed a frequency analysis of the oscillations, discovering that two dominant modes of oscillation exist: a low frequency and a high frequency. The low-frequency mode is reported to only occur for flow in transition and fully turbulent flows. The high-frequency mode is always observed.

Chyu et al. used transient liquid crystal technique to study the overall heat transfer coefficient in a channel with staggered array of indentations on the walls. A hemispherical shape and a tear drop shaped designs were studied. The authors could observe an enhancement of about 2.5 times the value obtained for a smooth-walled channel obtained by Dittus-Boelter correlation with a pressure loss of 50%.

Dimples are a very attractive option due to their low pressure drop feature, and part of the credit goes to its depression form as opposed to a protrusion which prevents it significantly from having form drag. This feature has made dimples to be found very useful in low pressure sections of turbine cooling system. Lienhart et al. in 2008 have conducted experiments to study friction drag on dimpled surfaces with turbulent flows. Authors concluded that the dimples do not lead to a drag reduction, supporting with results from experimental and numerical simulations, although there was no significant increase in pressure drop. Experiments conducted by Zhao et al. to study flow structures of dimples with relative depths h/d, with round or sharp edges concluded that there was no increase in friction factor observed with the presence of dimples. Mahmood & Ligrani have conducted flow visualization studies, investigating the influence of h/d, temperature ratio and Reynolds number on the flow structure and heat transfer performance of a dimpled channel. It was found that as h/d was decreased, the strength of local vortices increased, resulting in a net

augmentation of local Nusselt number values which were as high as 5 in some locations.

2.3 Recent Studies

Among the recent studies, Isaev et al. have presented results from numerical simulations on heat transfer enhancement by a spherical dimple on a wall in a narrow channel. This study focused on the influence of depth to diameter ratio and Reynolds number on the flow and heat transfer. The study concluded by stating that by increasing the dimple depth, there is a transition point which affects the structure of the flow, making it change from the stable, symmetric formations to unsteady, sweeping monovortex. This transition is accompanied by a significant increase in convective heat transfer in the downstream region of the dimple.

Dimple flows are being continuously investigated for about 2 to 3 decades now. They have contributed to a significant knowledge base on dimples, in characterizing a number of variations in the dimple parameters and essentially providing conclusive evidence of flow structures. It was thus concluded that the heat advected from a dimpled surface is higher than that of a flat surface of the same surface area as the foot print of the applied dimple. The mainstream turbulence was found to have a strong impact within the dimple feature than the walls of the channel around the dimple. As a result of such exhaustive studies, researchers concluded that

the heat transfer enhancement caused by the dimple indentation is caused by the advection of cooler mainstream fluid to the channel wall and this action was proved by the existence of fluid structures ejected from the dimple.

2.4 Present Study

The present work investigated and characterized heat transfer based on variations of dimple configuration in a narrow diverging and converging channel. Using a validated experimental setup, testing was performed over a range of Reynolds numbers specific to converging and diverging channel. All considered enhancements were placed in the blue region of Figure 2.1. More about this and other variations of this test section are discussed in the following chapters.

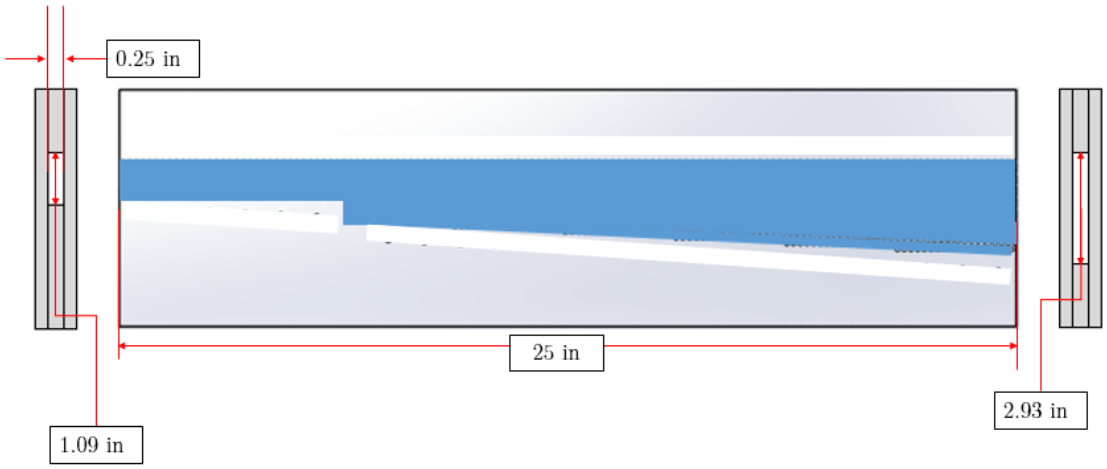

Figure 2.1: Geometric dimensions of the test channel.

3 Mechanism of Heat Transfer in Dimples

3.1 Introduction

Dimples or shallow cavitation are employed on surfaces exposed to fluid streams in many applications, including cylinders and spheres in cross-flow. It is well established from literature review that dimples reduce overall form drag. This occurs because the dimples cause the boundary layer on the cylinder to transition to turbulent much farther upstream, leaving a much smaller region of separated flow on the downstream region of the cylinder or sphere. Which is why, dimpled golf balls are much easily propelled over long distances than smooth ones. Dimpled surfaces are important in a number of internal flow applications. This is mainly because of the significant heat transfer enhancement they provide without substantial increase in pressure drop as when compared to other features like ribs and pins.

3.2 Flow over a Dimple

To better understand the effect of dimples, a discussion of the flow structure within the dimple is necessary. Important flow features in the presence of dimples are noted and described as follows – it is commonly observed that fluid gets drawn from above the dimple and gets united with the downstream part of the dimple. There are recirculation zones that exist in the dimple. Most studies confirm that the fluid in the dimple travels upward, out of the dimple giving rise to counter rotating

vortices that get stretched downstream. Fluid is replenished into the dimple from the sides to fill the ejected fluid and this process continues at certain frequency depending on many parameters.

3.3 Heat Transfer

Dimples may be formed in an infinite variation of geometries which results in various heat transfer and friction characteristics. The principle of cooling taking place inside the dimple, involves the phenomenon of flow separation over the surface. At sufficiently high velocities, the fluid stream detaches itself from the surface of the body, termed as flow separation. The location of the reattachment point depends on many factors like Reynolds number, surface roughness and level of fluctuations in free stream.

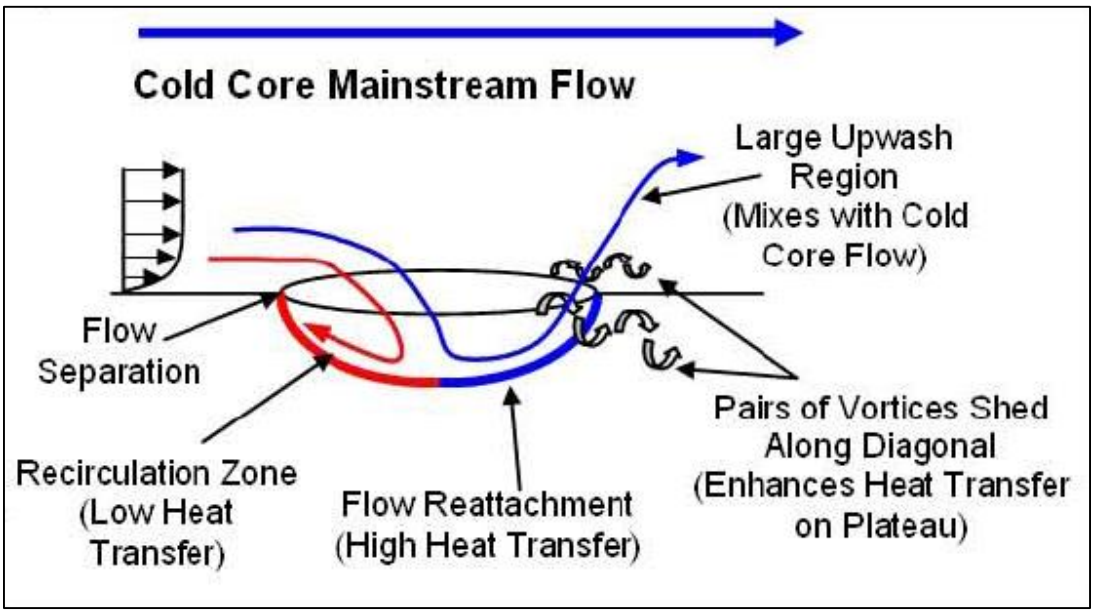

Figure 3.1: Principle of dimple feature as heat transfer enhancement.

The twin vortex structures produced by dimples are most prominent on the downstream of the dimple as well as the flat surface immediately downstream of the dimple. Figure 1 shows how flow passes over the dimple and the turbulence is created. The leading edge of the dimple works as a back-facing step and creates a low pressure region forcing the liquid inside the dimple. This region between separation and reattachment traps the fluid in recirculation, leading to low heat transfer characteristics. After the leading edge is passed, the fluid falls into the dimple impinging the inside surface of the trailing edge giving better mixing and higher heat transfer characteristics. This effect continues outside of the dimples to the upstream flat area, where the organized vortices formed inside the cavity, stretch outside drawing fluid out of the boundary layer to come in contact with the heated wall. The heat transfer reduces around the flat region since the vortices responsible for mixing lose strength. Some of these vortices leaving the dimple are responsible for thermal improvement in the contour around the dimple. Additional enhancement of heat transfer is found due to variation of the reattachment line caused by shear layer fluctuations. The hot fluid is driven out of the dimple in transverse direction and leave the dimple on one or both dimple sides depending on the instantaneous flow topology (symmetric or asymmetric). Surprisingly, the outcoming fluid is not

entering the following dimple as it might be expected, but due to its angle of outflow it moves directly into the main channel flow enhancing mixing process.

4 Choice of Measurement Technique

The main objective of this research is to investigate and understand a variety of heat transfer enhancement techniques over a wide range of Reynolds numbers. A transient liquid crystal technique will be used to gather detailed measurements. This technique is described in detail in a following section.

In comparison to other detailed measurement techniques, liquid crystals are most practical. An infrared (IR) thermography technique may be applied, however the windows are very expensive to provide data over the entire channel length. Typically, IR windows for the scale of this test section will cost over $20,000. The windows are also not practical as the enhancement features cannot be placed on such expensive windows.

Another technique is the use of naphthalene sublimation technique. The technique uses the heat and mass transfer analogy. Souza Mendes explains this technique in detail. A test section is machined and naphthalene is cast into the test section to become the walls. During testing, the naphthalene sublimates. Surfaces features (roughness) are measured before and after the sublimation to determine how the naphthalene sublimated. Data reduction is performed almost immediately to reduce effects of natural sublimation. Even though the results are contoured, the

process is very time consuming and tedious. Of these, the liquid crystal thermography is the most practical and cost effective for the heat transfer research.

5 Experimental Heat Transfer Rig

This research makes use of the stationary test rig. The stationary test rig is capable of taking stationary heat transfer measurements, offering a fast and easy setup to quickly provide analyses of stationary heat transfer tests. The following section provides a detailed description of the stationary test setup and how the test sections are designed and fabricated for the tests.

5.1 Stationary Heat Transfer Rig

The stationary heat transfer rig is shown in the Figure 5.1. Air is pumped through a hose connected to the building air supply. A gate valve is at the entrance of the rig, to control the mass flow of air entering the test section. The air passes through an orifice meter, to regulate the amount entering the test setup. The air enters a settling chamber, where the air slows down and settles to an even velocity distribution. After this, the air passes over a mesh heater. The mesh heater is connected to a DC power supply, such as an arc welder. An illustration of the mesh heater is provided in Figure 5.2. Through resistive heating in the thin stainless steel mesh fibers, the air gets heated before entering the test section. A sample temperature response is provided in Figure 5.3. Flanges are designed in such a way so as to fit any desired test section on to the stationary rig.

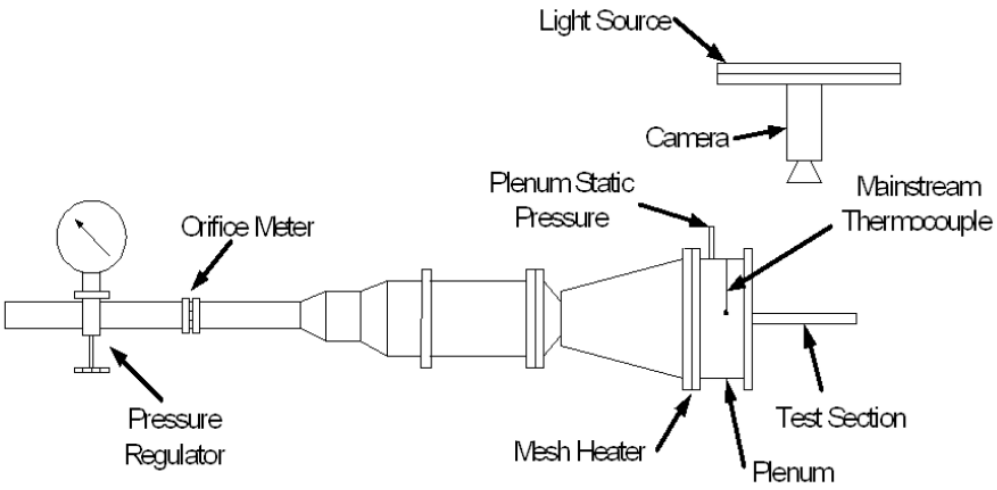

Figure 5.1: Schematic diagram of the stationary experimental setup

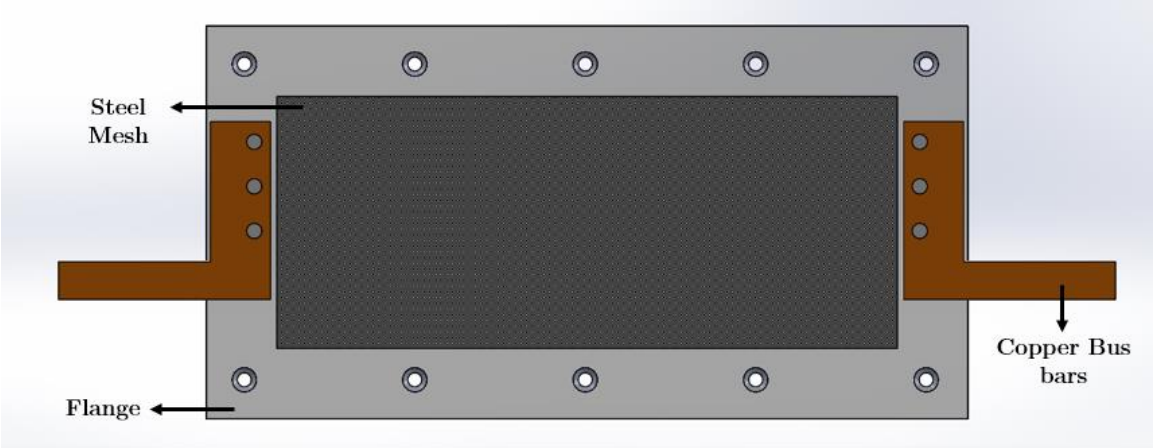

Figure 5.2: Mesh Heater.

5.1.1 Mesh Heater

The experimental method uses a transient liquid crystal technique. This needs a sudden injection of cold or hot fluid to cause a reaction in the liquid crystals. A mesh heater, as shown in Figure 5.2 provided by Dhungel in combination with arc welder. Gillespie et al. (1993) first measured the time response of a stainless steel mesh heater by coating the filaments with liquid crystal. To perform a test, the desired flow rate is set by an orifice meter. After setting the flow rate, the arc welder is turned on. Through resistive heating, the mesh almost immediately gets heated resulting in the air getting heated which passes through it. This generates an increase in mainstream temperature to suit the need of our experiment. The temperature change behavior is shown in Figure 5.3. The temperature change was measured with a *K*-type thermocouple.

The mesh heater component is made of Stainless Steel woven wire mesh with a 20 micron wire diameter. The free area of the mesh was about 32% which greatly reduced the free stream turbulence before entering the test section. Figure 4.2 shows the mesh heater fitted on to the flange. Since the mesh material is of low resistance, the power source utilized is of low voltage and high amperage power source. Power to the mesh is supplied by a Lincoln FLEXTEC™ 650 welder model. The welder provides a true step change in the temperature of the mainstream air.

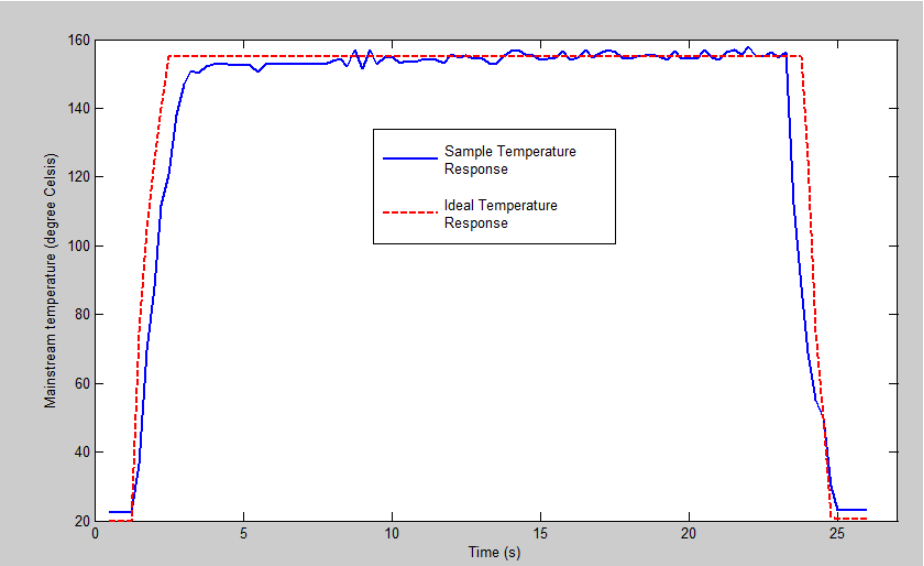

Figure 5.3: Temperature response.

The welder is operated constantly at a power of 140 to 160W to obtain the desired temperature change. The response time of the heater is almost immediate which can be observed with a change in color on the test section. The response time was found to be close to 10 milliseconds.

5.1.2 Baseline Test Section

The coolant channel is modeled in plexiglass[1] with no surface enhancements in the flow path for the baseline case. The test section is completely built in a modular fashion to aid quick and easy test section changes and troubleshoot routines. The test section is divided (not physically) into "narrow" and "wide" regions as shown in Figure 5.4 for identification reasons. The test section consists of a channel which is

[1] Transparent thermoplastic, often used as a lightweight or shatter-resistant alternative to glass. Although it is not technically a type of glass. *Source:* http://en.wikipedia.org/wiki/Poly(methyl_methacrylate)

diverging or converging depending on the type of flow intended to study. The test section is made of four plates: Top, bottom and two middle plates. The shape of the middle plates govern the shape of the coolant channel while the top and bottom plates set the height. As mentioned before, all these plates are made of Plexiglass and fixed together by screws to form one solid test section. The test section is mounted on a flange to enable a snug fit thereby preventing air leaks. This flange that houses the mesh heater is shown in Figure 5.2. This flange connects to the plenum by a series of hex nuts. The coolant flows from the plenum, through and out of the modelled channel. The transparent nature of plexiglass helps to see the color change through the top plate. Transient liquid crystal technique is used to determine heat transfer coefficient distributions on the baseline surface based on the response of color change due to the applied temperature change. The plexiglass plates are machined to the desired shape. The picture of the test section is shown in the Figure 5.4.

5.1.3 Inline and Staggered Dimple Test Section

The test section for inline and staggered configurations are very similar to the baseline set-up which was discussed in the previous section. The top and bottom plates are equipped with dimples and are machined to bring out a smooth finish. Arrangement of dimples dictate whether the test section is inline or stagger dimpled.

Figure 5.5 and Figure 5.6 show the representation of inline and staggered dimple patterns respectively. The dimples are fabricated only in the blue portion of the top and bottom plates as shown in Figure 5.4. Geometric details of these dimples are provided in Table 5.1. Iftikarahamad H. Patel et al. discussed these configurations and their ability to provide heat transfer enhancement.

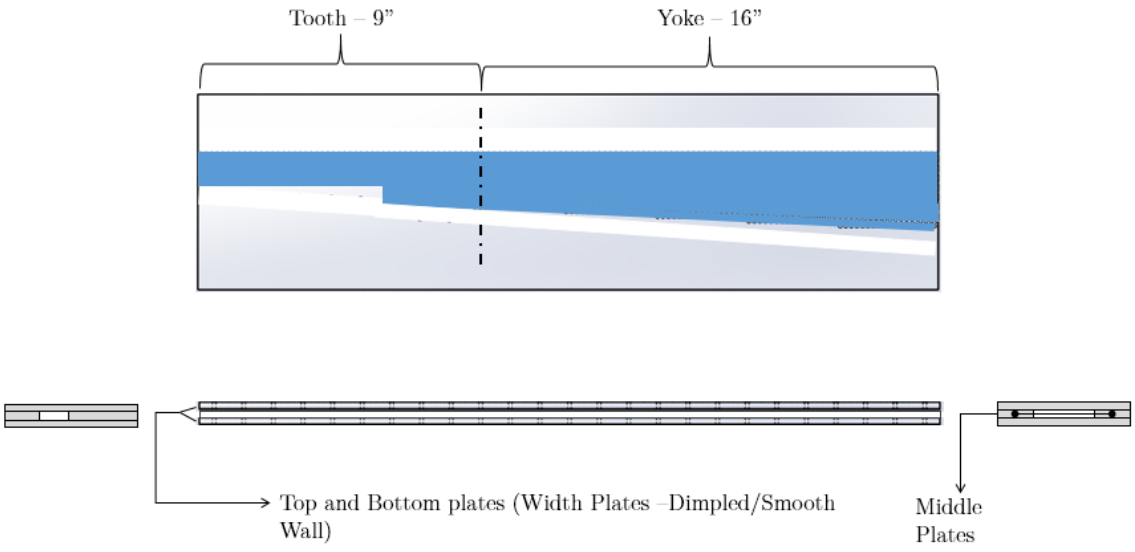

Figure 5.4: Test section of the coolant channel.

.

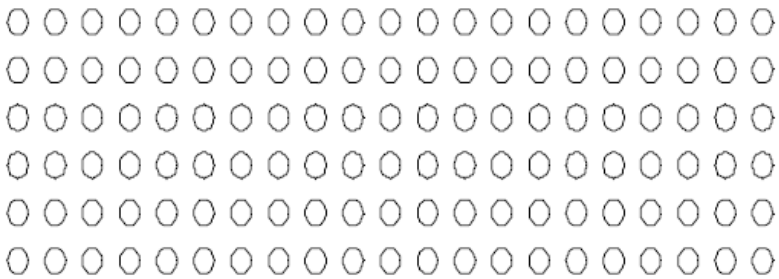

Figure 5.5: Inline dimples

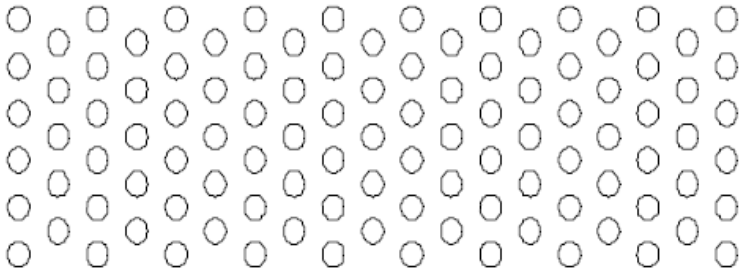

Figure 5.6: Staggered dimples

Type of dimples	x/d	y/d	Depth(δ)/d
Inline dimples 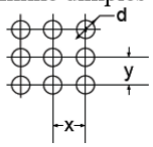	1.752	1.504	0.24
Staggered dimples 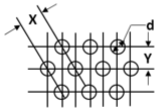	1.496	1.496	0.24

Table 5.1: Geometric details of the enhancement features used.

5.1.4 Camera Mounting

The camera used in this study is a Canon FS200, which has a CCD (charge-coupled device) chip for recording digital video. It is very compact and relatively inexpensive to buy and maintain. The camera is variable focus type. The camera is kept at a distance of approximately 2 *feet* from the test section to get the optimum resolution and complete view of the test section. This distance can be varied depending on the area of interest on the test section, since the camera is mounted on aluminum slot bars. In this study, the camera is placed at three different locations to view – the entire section, narrow area, and wide area. The mass of the camera is

$0.286kg$. The camera is secured to the aluminum slot bars by means of a C-clamp and sufficient care is taken to avoid a fall on the test section.

5.1.5 Light Mounting

Liquid crystal thermography requires a light source to view the changing colors of the liquid crystal. Liquid crystal data may be processed in two ways: a green start method or the hue calibration method. The first method is based on the Red, Green, and Blue (RGB) color classification system that is the default for many cameras and programs (like MATLAB). The RGB classification gives a value from 1-255 depending on how much red, green or blue is present in a particular pixel. On the other hand, the green start method makes a note of color change of a particular pixel, to know if it has attained a certain value of green. Based on this one pixel, the program makes an assumption that all the pixels begin at the same value of green and that the test area is evenly lit. This necessitates uniform lighting all across the test section because the value of green differs for different intensities of light. Even though the former method has the advantage of color purity separated from light intensity, it takes longer to post process. Since space is not a constraint on the stationary test section, the RGB method is more convenient. Two tube lights are mounted on the aluminum slot bar parallel to the camera. The lights must be placed in such a way so as to give uniform lighting to the test surface and at the same time

not reflect on to the camera lens from the plexiglass test section. Lighting system and the camera used are light weight making it easier for trouble shoot and adjustment routines.

5.1.6 Strategic (Sequential/Random) Addition of Dimples on the Test Section

The test section that was described in 5.1.2 and 5.1.3 was mainly intended to investigate about how a certain configuration of dimples could impact the heat transfer coefficient between the solid and fluid. Whereas, the main motive behind designing this test section was to explore an idea about varying the location of dimples in the region of flow.

This test section consists of a strategic combination of stagger dimple and smooth wall plates. The bottom plate of the test section is physically split into one section of narrow and four sections of wide regions to provide for combining strategically. The design of this test section is slightly changed to allow for the replacement of plates. Figure 5.7 shows the schematic of the design of this test section. Unlike the regular test section, the liquid crystal is painted on the bottom plate, and viewed through the top plate which is transparent. The middle plates form the shape of the channel (diverging or converging). The top, bottom and middle plates complete the coolant channel. Additionally, in this test section, there exists a support plate to provide bolster for the bottom plate which is split in parts. The

entire test section is clamped together, and enough care is taken to protect against air leaks. Since the idea behind designing this test section is to understand the effect of location of dimples, only the bottom plate houses dimple patterns (depending on the configuration), while the top plate remains smooth throughout.

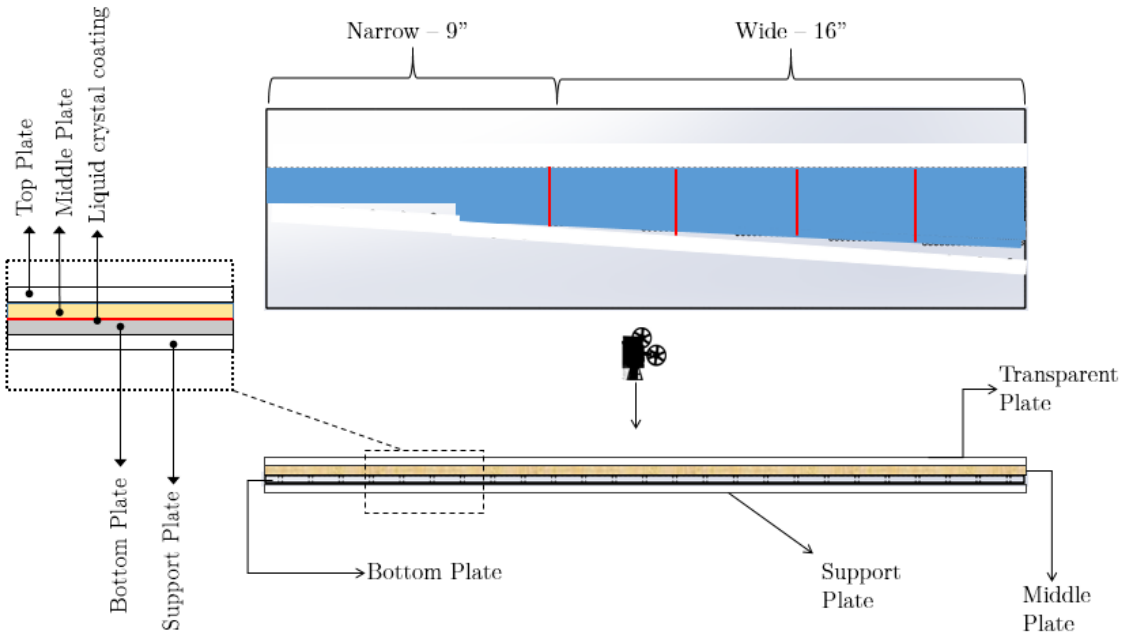

Figure 5.7: Schematic of the strategically dimpled test section.

6 Liquid Crystal Thermography

Liquid crystal thermography is one of the many ways to determine convective heat transfer coefficients of a surface of interest for cooling or heating applications. It has been mentioned in the first chapter about Newton's law of cooling where heat transfer coefficient is seen. A more suited form of Newton's law of cooling for the present study is given below,

$$q'' = h(T_m - T_w) \tag{6.1}$$

Where q'' is the heat flux of the surface, h being the heat transfer coefficient, T_m to be the bulk or mainstream fluid temperature and T_w is the temperature of the surface of interest. The heat transfer coefficient is a quantity that describes how well heat is exchanged from the solid to the bulk fluid. For complex flow conditions similar to which are considered in this study, the liquid crystal thermography provides a map of heat transfer coefficient on a surface of interest which is much harder to obtain through theoretical methods. This chapter talks about how liquid crystals have evolved to aid in heat transfer measurements.

6.1 Thermochromic Liquid Crystals

Liquid crystals are a unique substance which exist between solid and isotropic liquid phase of some organic compounds. It scatters incident light very selectively. The theory behind its optical characteristics involves the behavior of the molecular

structure. Each liquid crystal compound possesses a helical structure with a certain pitch length which are in the range of visible light wavelength. This length can be altered by changing the external stimulus – temperature and shear stress. The liquid crystal coating can respond repeatedly to the same physical changes since the basic chemical characteristic is unperturbed by applying stimulus such as temperature and shear stress. These liquid crystals are very similar to the liquid crystal displays used in watches and laptops, with the only difference being that displays respond to voltage. These elements consist of temperature sensitive (typically) elements containing microencapsulated Thermochromic Liquid Crystal TLC coated on a black backing. Each element changes color distinctly as its rated temperature is reached. Typically passes through a sequence – Tan, Green, Blue and finally black at a higher temperature. Such changes allow for qualitative and quantitative heat transfer information. Liquid crystals may be applied to the desired surface by using an airbrush.

Early studies with liquid crystals were unencapsulated which could produce some vivid colors. Atmospheric conditions and ultraviolet radiation could deteriorate and contaminate the liquid crystals leaving only a small time gap to perform experiments. To overcome this, modern forms of liquid crystals are found to be encapsulated in an alcohol binder after being coated with gelatin, which extends

their life from hours to years depending on the type of the encapsulation. The only drawback being the lack of vividness and color range.

6.2 Derivation of the Working Equation

The test plate is modeled as an infinitely thick slab under transient heat transfer phenomenon. Figure 6.1 shows a schematic of such a slab.

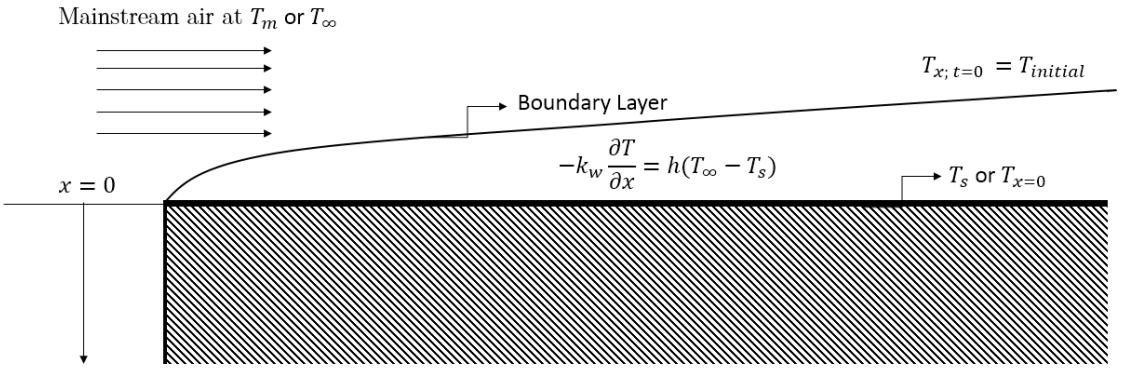

Figure 6.1: Schematic of flow over a semi-infinite slab

The slab is at a uniform temperature T_i at time $t = 0$. At time $t > 0$, the slab is allowed to interact with a stream of air at a different temperature. The mainstream of air provides a heat flux to the surface of the slab due to the temperature differential. This causes the phenomenon of convective heat transfer. Balancing thermal energy in the surface of the semi-infinite slab, and neglecting conduction along the direction of flow, the one dimensional heat equation is used to create a model,

$$\frac{\partial T}{\partial t} = \alpha \frac{\partial^2 T}{\partial x^2} \tag{6.2}$$

This assumption is made with the prior knowledge or calculation of a sufficiently high heat transfer coefficient, acceptable thermophysical properties of the fluid and wall, and sufficiently short test duration. Where T is temperature, t is time, x is the normal distance into the solid, and α being thermal diffusivity of the solid material. It is assumed that the surface is infinitely thick, so that heat conducts predominantly in one direction. Boundary condition of $T = T_i$ at $t = 0.$ and a convective boundary condition is applied to the surface,

$$-k_w \frac{\partial T}{\partial x} = h(T_\infty - T_s) \tag{6.3}$$

Where k_w is the thermal conductivity of the solid material, the left hand side of the equation represents Fourier's law of conduction and the right side, Newton's law of convective cooling. The boundary conditions show the coupling of conduction within the solid material and convection due to a fluid flowing over it. Solving the partial differential equation with the prescribed boundary conditions, gives the

transient response of the test plate wall due to the convective heat load applied by the mainstream air.

$$\frac{T(x,t)-T_i}{T_m-T_i} = erfc\left(\frac{x}{2\sqrt{\alpha t}}\right) - \exp\left(\frac{hx}{k_w}+\frac{h^2\alpha t}{k_w^2}\right)\left[erfc\left(\frac{x}{2\sqrt{\alpha t}}+\frac{h\sqrt{\alpha t}}{k_w}\right)\right] \quad (6.4)$$

This equation describes the temperature on the surface and into the solid as a function of x for a given bulk temperature, T_m. Liquid crystals are applied to the surface of the solid, that is at $x = 0$. Hence, equation 6.4 reduces to -

$$\frac{T(0,t)-T_i}{T_m-T_i} = 1 - \exp\left(\frac{h^2\alpha t}{k_w^2}\right)\left[erfc\left(\frac{h\sqrt{\alpha t}}{k_w}\right)\right] \quad (6.5)$$

Equation 6.5 is the mathematical model for liquid crystal thermography. As far as the problem goes, only temperature of the surface varies with time. If a fluid flows at time $t = 0s$, the heat transfer coefficient (h) can be iteratively solved. The term $T(0,t)$ is monitored, and attained by liquid crystal thermography by relating the color reflected off the liquid crystals painted on the wall.

The derivation of the heat conduction solution involved the assumption of test model to be infinitely thick. This translates into saying that, the test plate is a thick wall in which one end is exposed to a temperature different from itself and the other end is not affected by this condition. The thermal pulse generated at one boundary does not reach the other end or rather, it takes an “infinite” time to reach

the other end. It is the material property called thermal diffusivity (α) that dictates the time it takes to reach the other end. An assumption as follows is taken as a condition or a limiting factor for the semi-infinite condition to hold good. This assumption is valid as long as the thermal penetration due to conduction does not extend to cause 2-D conduction effects.

$$t_{max} = \frac{D_p^2}{\alpha} \tag{6.6}$$

Where t_{max} is the maximum testing time, D_p is the target plate thickness, and α is the thermal diffusivity of the plate. Ideally, a material of very low diffusivity is desired to increase the maximum time available for testing. Hence, plexiglass is chosen which has a thermal diffusivity (α) value of 1.09e-7m^2/s.

6.3 Experimental Procedure

This section describes the various steps involved in carrying out the experiment – the application of liquid crystals on the surface of interest, calibration, testing conditions, and post processing.

6.3.1 Material Choice and Liquid Crystal Application:

As mentioned before, liquid crystals are applied to the test surface with an air brush. Since the study focuses on heat transfer characteristics along the channel, the liquid crystal needs to be viewed through the material. Hence, optically clear

materials need to be chosen. Clear acrylics such as plexiglass or lexan are chosen due to their optical clarity.

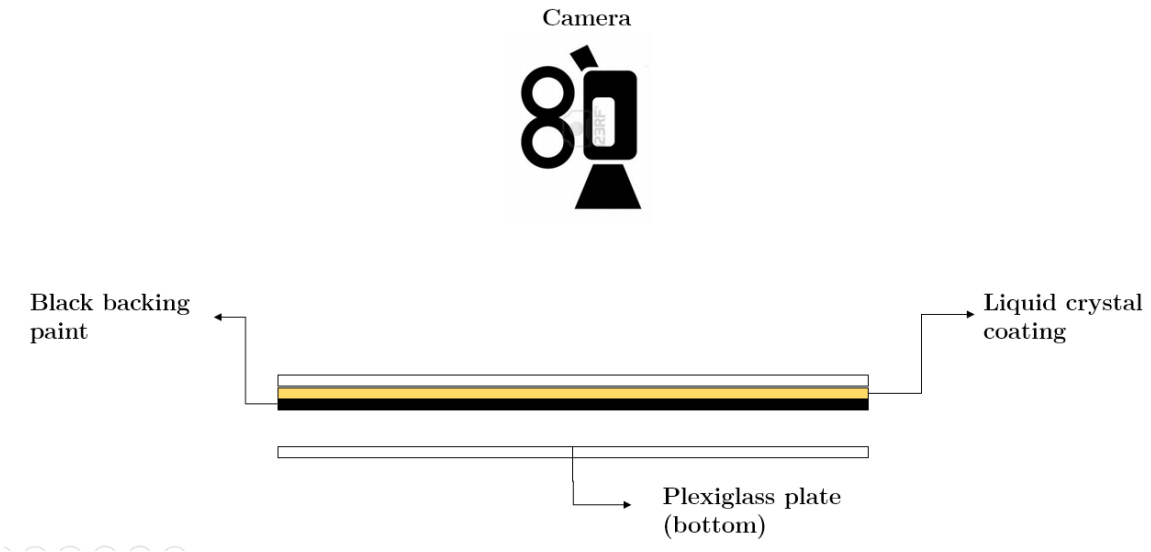

Figure 6.2: Illustration of location of liquid crystal, black backing and plexiglass with respect to camera for study of dimples on regular test section.

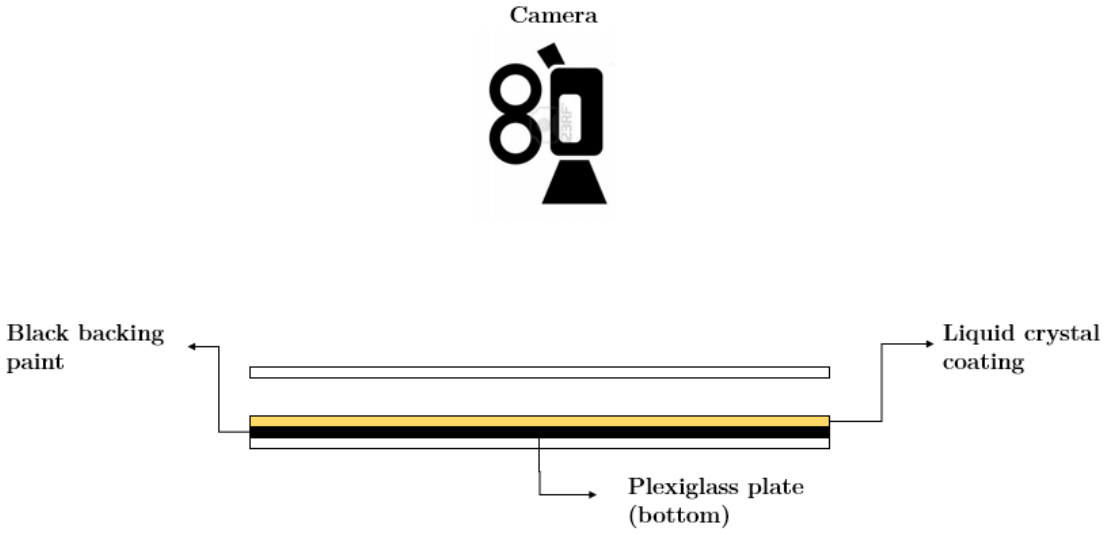

Figure 6.3: Illustration of location of liquid crystal, black backing and plexiglass with respect to camera for sequential/random addition of dimples on test section.

The methods followed for application of liquid crystals in this study, are shown in Figure 6.2 and Figure 6.3. Figure 6.2 shows the liquid crystal application configuration used when the regular test section is employed for study. The top plate is applied with liquid crystal first and then a uniform coat of black backing is provided. Figure 6.3 shows the liquid crystal application configuration used for the strategic dimpled test section. The bottom plate is painted with a uniform coat of black backing followed by a coat of liquid crystal. It is evident from both these configurations that the liquid crystal coating must remain closest to the camera.

According to Cooper & Field, typically, the thickness of liquid crystal is in the order of $50\mu m$. In this present study, the coating is not measured for thickness, but liquid crystal is applied on the material until it appears cloudy on the surface to view through. On this, a black backing is applied to provide better contrast of the liquid crystals under light. The thickness of this black backing is similar to that of liquid crystals and the coating is considered sufficient when no light is visible through the test section.

For the present study, acrylic glass is extremely ideal for to the principle followed (1-D semi-infinite heat conduction with convection at the boundary) due to the low thermal diffusivity (α). Since the tests are transient, the maximum testing time due to the limiting factor (6.6), poses a constraint. Therefore, the low thermal

diffusivity reduces the conduction effects of the experiment, producing only convective heat transfer results.

6.3.2 Testing

Liquid crystal thermography uses changes in colors reflected by the liquid crystal to infer surface temperatures. A video camera is used to capture the light reflected over time, as shown in Figure 6.4. Thermocouples are used to capture the temperatures of the bulk fluid throughout testing at a quick rate. In the present study, two thermocouples are placed in the channel of test section – one at the entrance and one at exit. The bulk fluid temperature would be interpolated for all the local points in between inlet and exit. Depending on the area of interest, there would be an

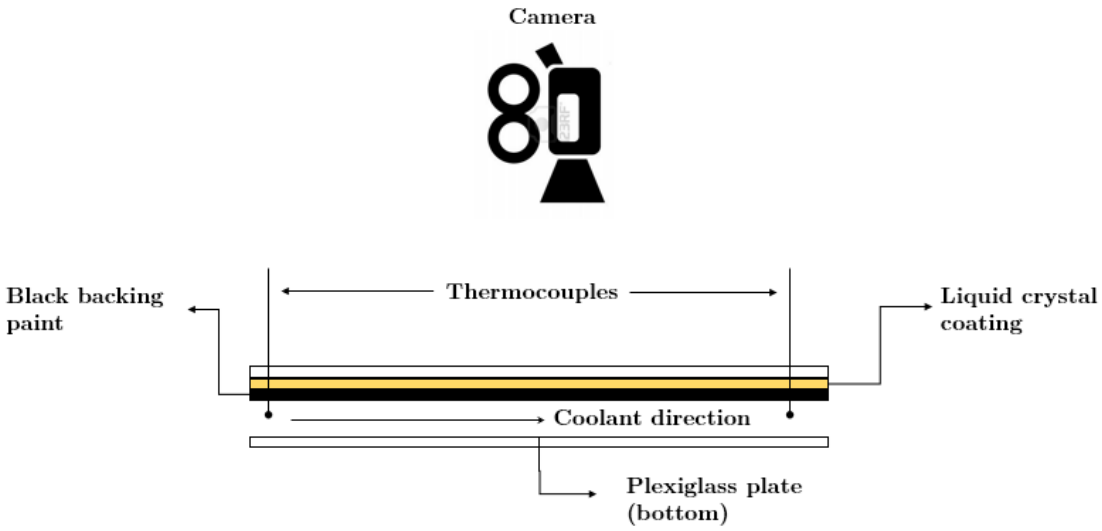

Figure 6.4: Illustration of the location of thermocouples in the test section

additional thermocouple to read bulk temperature at that point. The step change would be induced in the test by the mesh heater as described in the previous chapters.

6.3.3 Testing Conditions

A transient test is performed once the liquid crystal is applied and setting up of test section is done. It has been established that the surface temperature i.e. $T(0,t)$ changes with time at any given constant mainstream temperature (T_m) as shown in equation 6.5. When $t = 0$, a step change in the mainstream temperature (T_m) is

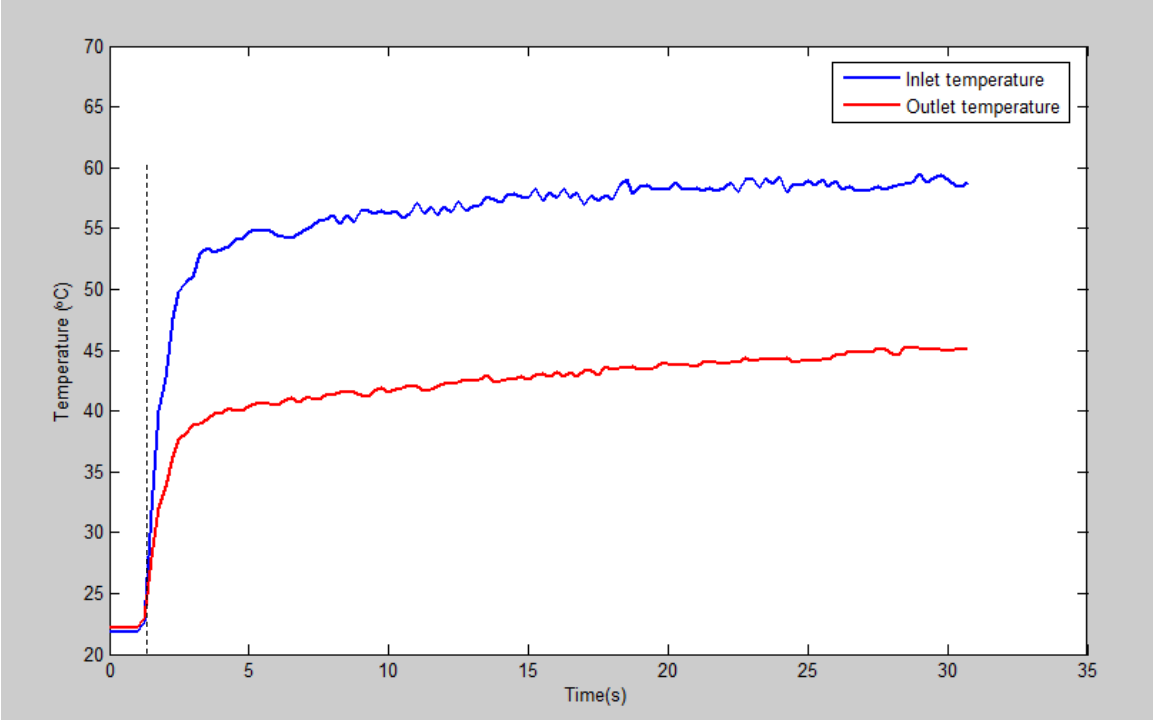

Figure 6.5: Step change in inlet and outlet temperatures.

introduced, as shown in Figure 6.5. A video camera is used to record the response of liquid crystals to the applied temperature change.

Induction of a steady color change in the liquid crystals is achieved by choosing an appropriate mainstream temperature. Since the current study focuses on stationary experiments, the bulk fluid temperature is insignificant as long as it induces an appreciable color change in the liquid crystal. It is important to note that although the step change is induced a second or so later, it is trimmed to synchronize with the video during post processing.

6.3.4 Calibration of Liquid Crystals – Wall Temperature Calculation:

The temperature of the surface being examined is required in order to calculate the heat transfer coefficient from equation 6.5. The temperature is read from the video of the color change of the liquid crystal due to an applied mainstream temperature. This study employs a "Green Start" method for calibrating liquid crystals with a k type thermocouple. It is called "Green Start" because, in the color band, green is the color which is most dominant. In this method, the calibration thermocouple is used to find a temperature corresponding to the appearance of green on the surface. The thermocouple is placed on the surface with the liquid crystal coating to measure wall temperature over time. Sufficient care is taken to ensure the bead of the thermocouple remains on the surface, and not bent upwards measuring

mainstream temperature. The camera is focused for clear visibility of the location of thermocouple as shown in Figure 6.6. The video stores the information on how much red, green and blue (RGB) light is present on a scale of 0-255. If R=0, G=0, and B = 255, then the pixel is blue. If R=255, G=0, and B=0, the pixel is red. Mixtures of RGB values produce different colors and shades. The color of the surface is black before applying a change in mainstream temperature, corresponding to a certain green value, since a true black surface does not exist in nature (ideal black RGB values = 0). The surface needs to be illuminated uniformly such that the background intensity of the color on the test surface is constant. When a temperature is applied, the color on the surface changes which is recorded along with time, and temperature of this surface is monitored by the thermocouple. The time is correlated on the temperature curve to obtain the actual appearance of green. Maximum background intensity for a color (green in this study) is called threshold. Although, in the transient experiment, the threshold value is set in such a way so that a sufficient increase in local pixel intensity is observed and recorded only if it passes this threshold value, implying that the color change has occurred. Then, the time it takes to reach this threshold value (temperature) by every other pixel on the surface is recorded for analysis.

Figure 6.7 shows the change in color green corresponding to temperature. The calibration region starts when the color changes from red to green. The location of thermocouple for calibration is chosen carefully. As the thermal diffusivity of the liquid crystal, black backing, plexiglass wall and thermocouple bead are different, and if the thermocouple is placed in a region of high heat transfer, the materials

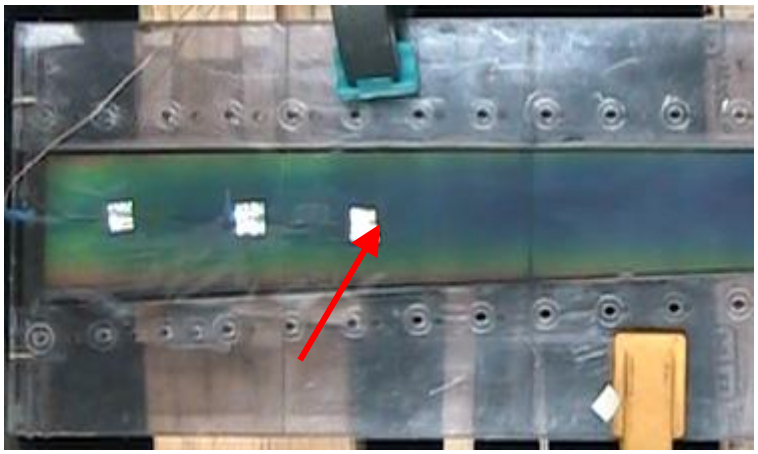

Figure 6.6: Location of thermocouple for calibration.

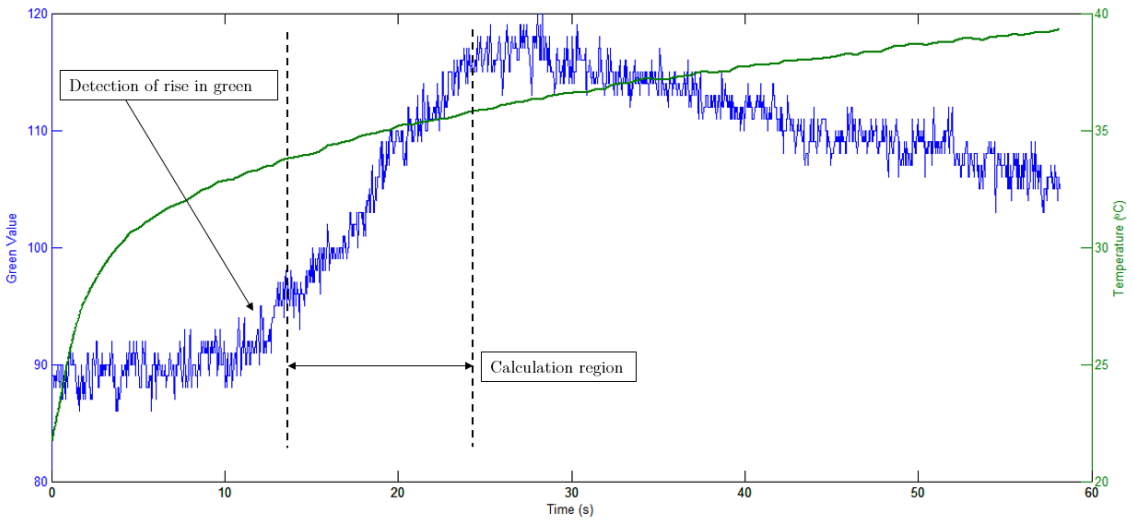

Figure 6.7: Temperature and green color correlation

heat up at different paces, making the calibration inaccurate. When steadily heated, the rise or drop in temperature is more uniform, showing better calibration of liquid crystal colors to temperatures.

6.4 Data Reduction Procedure

The video of the liquid crystal color change and temperatures of bulk and wall are recorded. The data is imported into a MATLAB code which reduces the recorded data into heat transfer coefficient map. This section talks about the entire information extraction process after the experiment is complete.

6.4.1 Setting Up for the Reduction Process

The recorded video is trimmed in size and running length. The video's starting point is trimmed to coincide with the step change input of the mesh heater. For every test, an audible cue is created to indicate the induction of step input. During the video trimming routine, this cue is made to be $t = 0s$. The video is trimmed in size so that the program can only work on the region of interest, cutting out the extraneous pixels which would otherwise be used in the heat transfer coefficient calculations impacting the accuracy of the solution. A rotation option is included in the code to account for any tilt in the camera's view while recording the video. Along with the video, even the thermocouple data is trimmed to match the start point of the video, which in turn aligns with the step change. At this phase, a video containing

the information of color change of every point (pixel) on only the test surface from the instant of start of the mesh heater to stop is created. Figure 6.8 shows a sample frame which is trimmed in size to time.

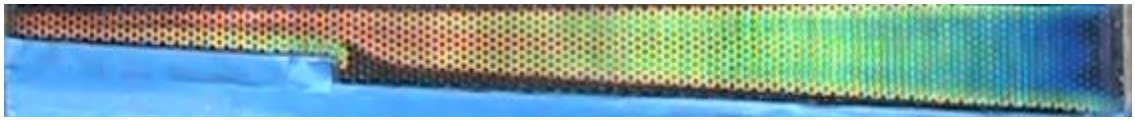

Figure 6.8: Sample trimmed frame of the video ready to be fed into the analysis program.

6.4.2 Robust Analysis Procedure

Once the time required to reach $T(0,t)$ is known for every pixel on the surface being examined, the equation 6.5 has only one unknown, i.e. h. This implies that only one wall temperature and time pair is needed to solve the equation to attain heat transfer coefficient (h). In order to reduce errors, data is collected over the entire range of liquid crystal color change and test duration. In the transient experiment, the threshold value is set in such a way, that the local pixel intensity reaches or exceeds the threshold implying that the color change has occurred. Since the program records the time it takes to reach this temperature by every other pixel on the surface, the program captures only those pixels which show a change in color or intensity eliminating extraneous data and saving ample computation time. An $fminsearch$ (MATLAB) function is used which finds the minimum of a scalar function of several variables, to find the value of h by minimizing error. Figure 6.9

shows how the value of h is chosen corresponding to a minimum value in error for an arbitrary pixel on the surface of interest. It can be seen that the error is not zero for the chosen h value due to associated numerical errors.

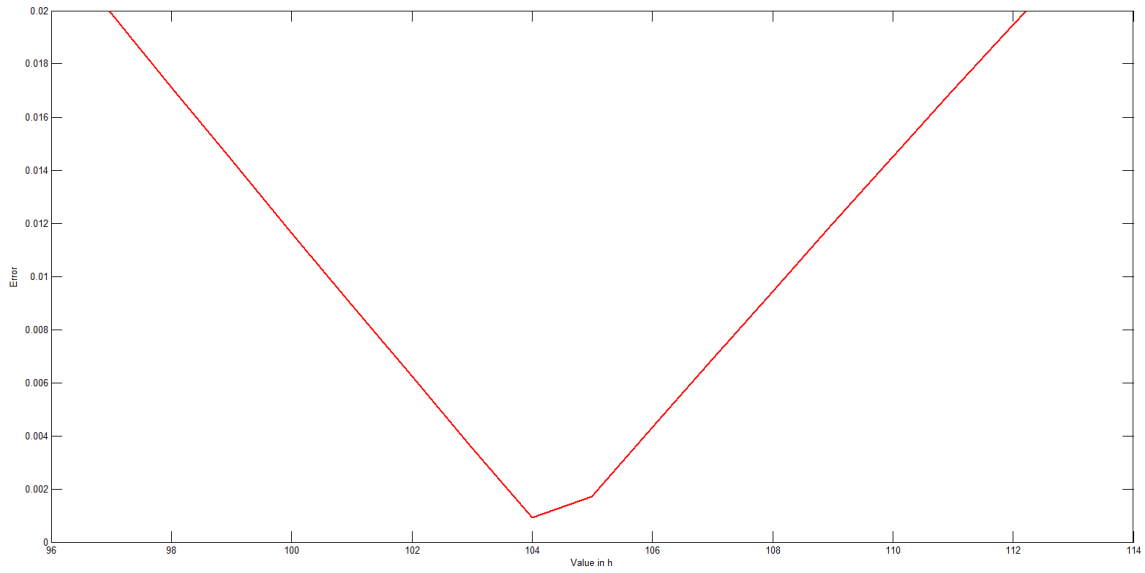

Figure 6.9: Plot of error versus h with the *fminsearch* optimization function.

6.5 Post Processing

Every pixel in the surface of interest is converted into a map of heat transfer coefficient. The MATLAB program displays the detailed results as shown in Figure 6.10. The code has the capability to compute local area averaged heat transfer coefficients as per user's choice.

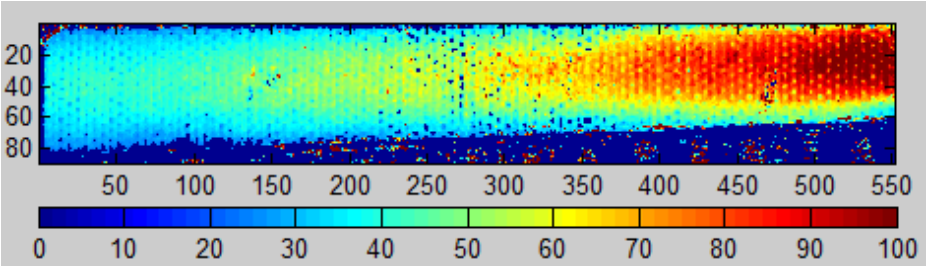

Figure 6.10: Sample result of the post processing routine that gives out heat transfer coefficient map.

6.6 Uncertainty

There are various factors that can affect the liquid crystal thermography results, such as bandwidth, the color imaging processing techniques, coating thickness, quality of the thermographic liquid crystal coating, lighting angle, etc. To quantify the amount of uncertainty present in the final calculation of h, all sources of uncertainty need to be explored - $T(0,t), T_i, T_m, \alpha, k_w$ *and* t.

6.6.1 Instrument Uncertainties

In the experimental set up, the orifice metering device has a precision of two decimal places. Due to which, the Reynolds number has an uncertainty of ± 60. Throughout the test, k type thermocouples are used which have an uncertainty value of $\pm 1.2°C$. The temperature associated with the test section ranges from an initial temperature of T_i to a final temperature. Due to this reason, average values of α and k_w are used. These properties of materials change with temperature, hence the uncertainty.

6.6.2 Calibration Uncertainties

Liquid crystal thermography is used to read off the temperature of the surface. This temperature is determined by relating the liquid crystal color change to a temperature indicated by a thermocouple placed on the surface. This process has quite a bit of uncertainty associated with it. The uncertainty associated with thermocouple, uncertainty due to the liquid crystal and black backing thermal conductivities, uncertainty associated with the camera in determining red, green and blue values, etc. Since the camera records the amount of color in integers from 0 to 255, an uncertainty of ± 1 is assumed. Importantly, the time step for thermocouple and frame rate of camera also have a degree of instrument uncertainty. Since the time step of the data acquisition system is one quarter of a second, the uncertainty associated with it is 0.125s. The camera shifts a frame for every 0.033s, which in turn produces an uncertainty of 0.0165s.

6.6.3 Overall Uncertainty

Uncertainty is an integral part of the design and analysis of liquid crystal experiments. Care must be taken to minimize the uncertainty to the maximum. Liquid crystals may be created to read temperature changes ranging from $2°$ to $100°C$. Choosing a temperature range is very critical in the liquid crystal

thermography, mainly so that the color change can be captured with as much detail as possible.

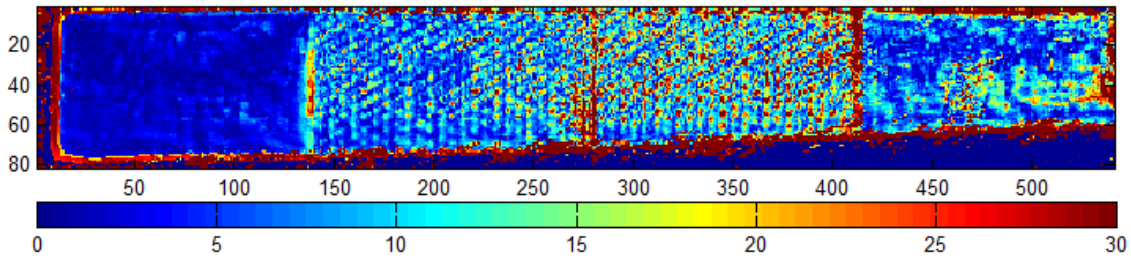

Figure 6.11: Overall uncertainty/errors associated with the experiment.

Figure 6.11 shows the plot of overall uncertainty associated with the experiment. One of the cases from increscent/strategic configurations are considered for the study. The study incorporates uncertainties corresponding to the thermocouple, set green threshold value for attaining wall temperature history, thermal diffusivity and conductivity of the surface, and Reynolds number. All the uncertainties were assumed to be independent and added in quadrature for every pixel to attain a whole plot. The overall uncertainty on an average turns out to be around 14.47%. Most of the uncertainty remains along the edges of plates and test section, possibly due to the vibrations.

Table 6.1 provides the breakup of the components associated with the overall uncertainty that is shown in Figure 6.11. The reference conditions are arrived at by averaging multiple runs with same parameters. Of all the parameters, change of 5% in thermal conductivity of the wall produces an error or uncertainty of approximately

6.1%. Altering the calibration value of green, provided a lower heat transfer coefficient since each pixel takes longer time to reach the increased threshold value. The green threshold value is originally fixed based on experimental results. Change in Reynolds number yields a value that is off by 1.2% from reference conditions. It should be noted that the variation in thermal conductivity (k_w) is the largest contr-

Parameter	Value of $\boldsymbol{h}$ in $\boldsymbol{W/m^2K}$.	**Uncertainty** (%)
Reference conditions.	57.657	--
Increase of one unit in green value threshold.	56.388	2.204
Upper bound uncertainty of thermocouple.	58.4764	1.345
5% increase in α	56.926	1.267
5% increase in k_w	61.1706	6.094
Variation of 100units in Reynolds number	58.994	2.32

Table 6.1: Table of uncertainties

ibutor to the overall uncertainty.

6.6.4 Choice of Temperature Band of the Liquid Crystal

The range of Reynolds number (Re) to run the air through the test section is known before the beginning of experiments. This enables the user to predict the temperatures the test section would experience with the aid of thermocouples. The maximum time of the test is restricted by equation 6.6. Ultimately, the time of the test is dictated by the step change of the mainstream temperature. In this study, a

mesh heater is used as explained in 5.1.1. The step mainly depends on the power settings of the source used to supply power to the mesh heater and also the mass flow rate. Knowledge of the heater response at expected flow rates, prior to the inception of actual study is very crucial. A k type thermocouple is placed on the surface to examine the surface temperatures at expected mass flow rates, at three different regions – the entrance, midsection and exit, to monitor the range of temperatures at these locations to estimate the band of liquid crystal that would be needed. The knowledge of Reynolds number (Re) enables the user to estimate the heat transfer coefficient by the virtue of Dittus-Boelter equation,

$$Nu_{db} = 0.023Re^{\frac{4}{5}}(Pr)^{\frac{1}{3}} \tag{6.7}$$

Where Nu_{db} is the Nusselt number, given by,

$$Nu = \frac{hD_H}{k_f} \tag{6.8}$$

Where h is the heat transfer coefficient, D_H is the hydraulic diameter and k_f is the thermal conductivity of the fluid.

7 Results and Discussion

Local data from the channel surfaces are reported for understanding of the local flow phenomena and additionally to gain an extensive understanding of heat transfer coefficient from the surface of the channel. These data are averaged across the pixels in span-wise direction and plotted on the channel. Data from baseline and dimpled configurations provide a valuable comparison between two experiments.

Three flow rates were explored for each of the following flow configurations on the stationary rig for the baseline and dimpled test sections. Bulk fluid temperature thermocouples are placed at the inlet and outlet of the channel of each test section to capture the temperature data for analysis. Heat transfer is based on the local fluid temperature, therefore locations between the inlet/outlet have linearly interpolated mainstream temperatures. It was found experimentally and confirmed with CFD that the fluid temperature has a linear drop in temperature. Local fluid temperatures in the test section are found using the same linear interpolation technique.

7.1 Diverging Flow Configuration

Figure 7.1 shows the direction of flow in the test sections used for this configuration. Reynolds numbers of 7000, 14000 and 28000 are explored.

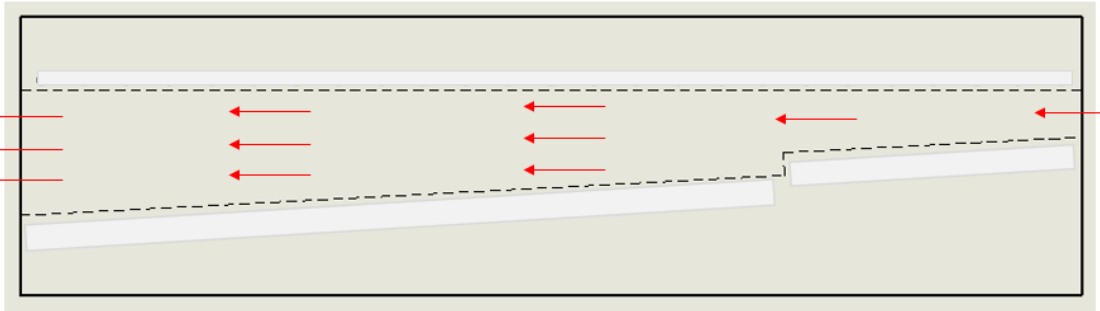

Figure 7.1: Representation of the diverging flow direction.

Table 7.1, Table 7.2, and Table 7.3 show heat transfer contours and pressure drop details for a Reynolds number of 7000, 14000, and 28000 for all the test sections, respectively. As indicated in Figure 7.1, flow enters the channel from the left side, and exiting from the right. The baseline results are used for comparison of all proceeding heat transfer enhancement geometries. The heat transfer is significantly higher in the entrance region due to strong acceleration of flow into the narrow channel from the plenum. As the flow develops into the channel, the heat transfer drops rapidly and becomes non-uniform. Inline and Stagger dimple geometries that are studied should provide higher heat transfer than the baseline case. The overall average heat transfer coefficient for the baseline based was measured to be around 80 for narrow and 20 for the wide region. The smooth tube correlation (based on Dittus-Boelter) for the Nusselt number based on inlet hydraulic diameter provides similar levels. However, in this study, the baseline value is lower as the flow deceler-

Reynolds Number and Case	Heat transfer Coefficient, h, (W/m^2K)	Pressure drop ratio	Heat transfer enhancement ratio	Heat transfer contour
Re 7000 – Baseline	80.10 (T); 19.5 (Y)	1	1	(Wide) 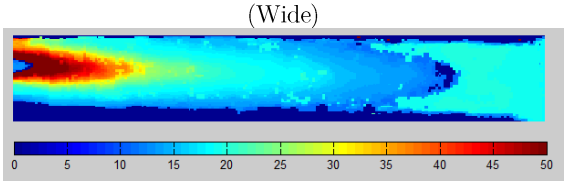 (Narrow) 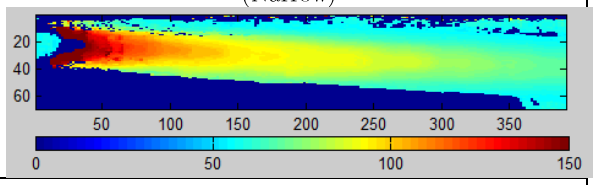
Re 7000 – Inline dimpled	108.4(T); 32.3(Y)	1	1.353(T); 1.65(Y)	(Wide) 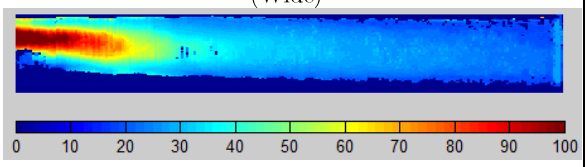 (Narrow) 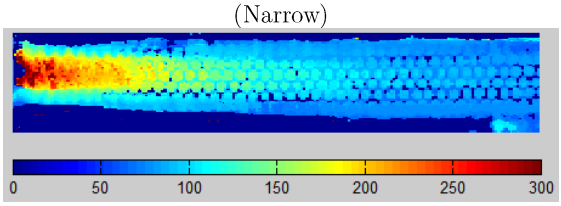
Re 7000 – Stagger dimpled	120.54(T); 28.1(Y)	1	1.504(T); 1.44(Y)	(Narrow) 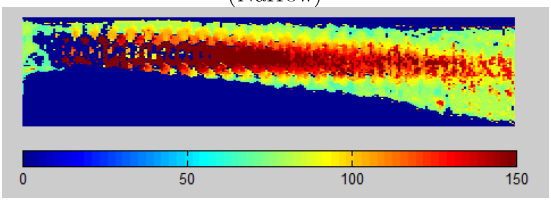 (Wide) 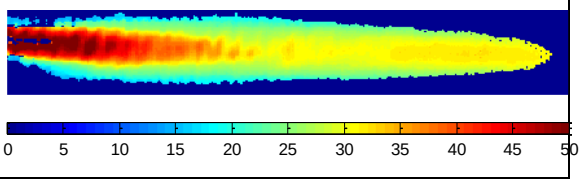

Table 7.1: Results for diverging flow configuration - Re 7000 (T – narrow and Y – wide)

ates inside the diverging channel and reduces overall heat transfer.

Reynolds Number and Case	Heat transfer Coefficient , h, (W/m^2K)	Pressure drop ratio	Heat transfer enhancement ratio	Heat transfer contour
Re 14000 – Baseline	148.6 (T); 42.8 (Y)	1	1	(Narrow) 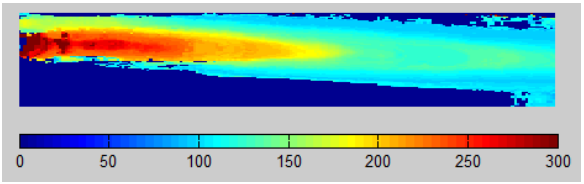 (Wide) 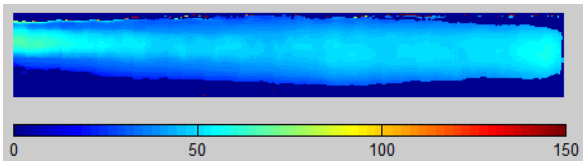
Re 14000 – Inline dimpled	154.5(T); 45.36(Y)	1	1.039(T); 1.06(Y)	(Wide) 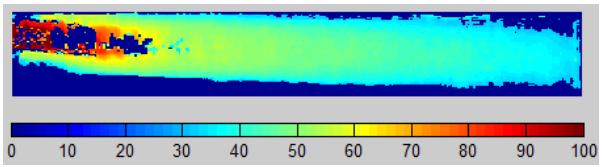 (Narrow) 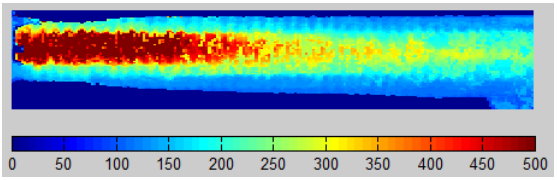
Re 14000 – Stagger dimpled	296.12(T); 59.3(Y)	1.16	1.504(T); 1.38(Y)	(Narrow) 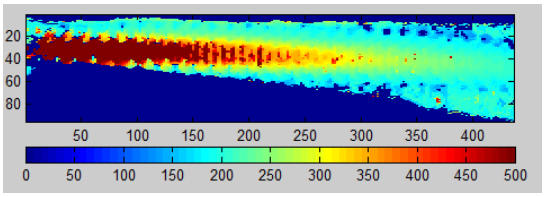 (Wide) 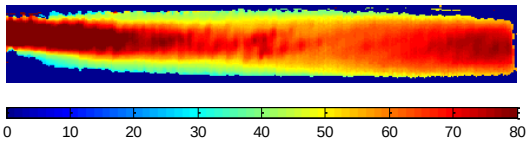

Table 7.2: Results for diverging flow configuration - Re 14000 (T – narrow and Y – wide)

Reynolds Number and Case	Heat transfer Coefficient, h, (W/m2K)	Pressure drop ratio	Heat transfer enhancement ratio	Heat transfer contour
Re 28000 – Baseline	387.7 (T); 175.17 (Y)	1	1	(Narrow) 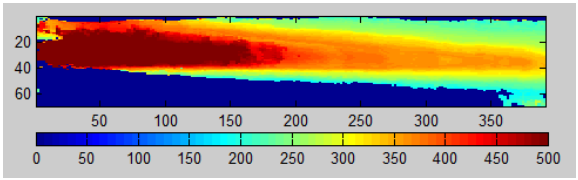 (Wide) 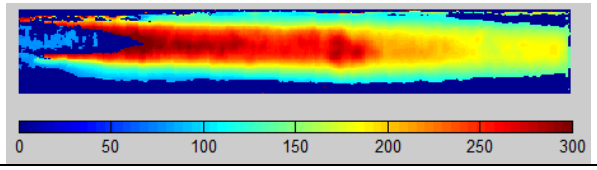
Re 28000 – Inline dimpled	670.4(T); 227.4(Y)	1.1	1.73(T); 1.3(Y)	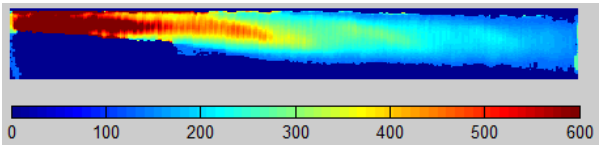
Re 28000 – Stagger dimpled	803.1(T); 246.74(Y)	1.271	2.07(T); 1.41(Y)	(Narrow) 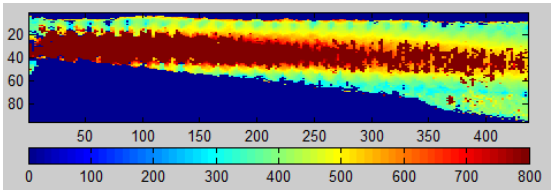 (Wide) 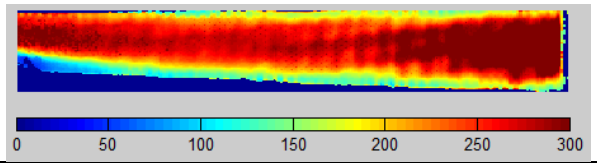

Table 7.3: Results for diverging flow configuration - Re 28000 (T – narrow and Y – wide)

Heat transfer performance is relatively high in the narrow region because of the entrance effects in addition to the accelerating effect of the flow due to the divergence in section. As the channel Reynolds number (Re) is increased, an increase in nonuniformity is observed due to the sharp contrast in convective heat transfer taking place between the stagnation and recirculation zone within the dimple. It has been explained in Chapter 3 that the recirculation zones are known to characteristically have low convective coefficients. The flow in the recirculation attains the temperature of the wall, reducing the heat transfer between flow and wall.

It can be seen in the case of diverging flow, that the heat transfer augmentation with staggered dimples is significantly higher when compared to inline dimples. As the arrangement of the dimples become more scattered, the flow disturbance is increased resulting in an increase in heat transfer. This augmentation is believed to occur due to the interaction between the twin vortices between dimples which is lesser to an extent in the case of inline dimples due to a certain fashion of orderliness associated with it. This is also one of the reasons why the pressure drop is higher for the case of stagger dimples, as the flow is more turbulent and mixed as compared to inline dimples.

7.2 Converging Flow Configuration

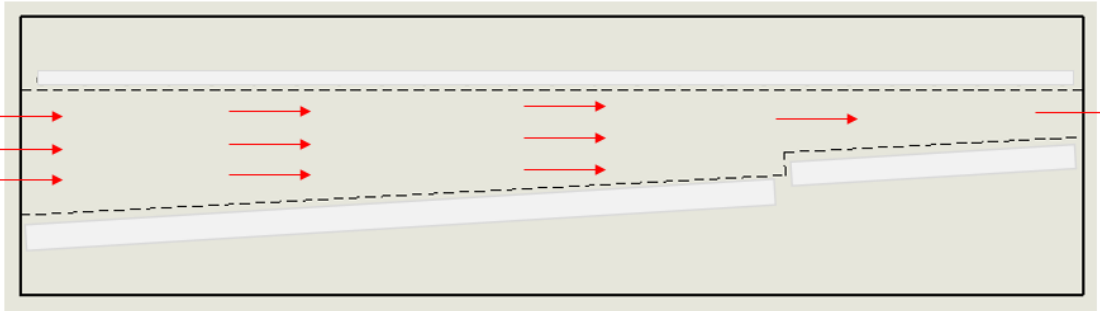

Figure 7.2: Representation of the converging flow direction.

Table 7.4, Table 7.5, and Table 7.6 show the heat transfer and pressure drop results for the Baseline, Inline dimpled and Stagger dimpled cases. Three Reynolds numbers of 3500, 8900 and 18000 are explored for the converging flow configuration.

The heat transfer plots in Table 7.4 shows that there seems to be a steady increase in heat transfer coefficient for Reynolds number 3500. The pressure drop was almost constant for all the run cases. The plot for staggered dimpled case are split into narrow and wide region mainly for better resolution of data, and also because the narrow and wide regions require different heat settings to observe a color change.

Since the Reynolds number is low (Re = 3500), the inertial forces play an important role in determining the heat transfer and the flow field. The presence of staggered or inline dimples has a visible effect on the heat transfer through the channel. In general,

for the converging flow case, the narrow region of the channel has higher heat transfer characteristics due to the converging effect that the channel imposes on the flow,

Reynolds Number and Case	Heat transfer Coefficient, h, (W/m^2K)	Pressure drop ratio	Heat transfer enhancement ratio	Heat transfer contour
Re 3500 – Baseline	36.5 (T); 32.5 (Y)	1	1	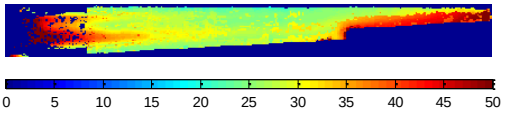
Re 3500 – Inline dimpled	45.4(T); 36.8(Y)	1	1.24(T); 1.13(Y)	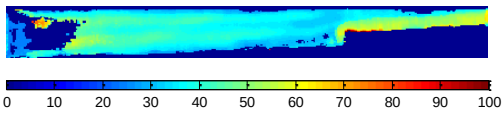
Re 3500 – Stagger dimpled	49.77(T); 41.63(Y)	1	1.36(T); 1.28(Y)	(Narrow region) 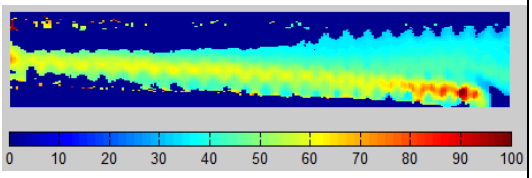 (Wide region) 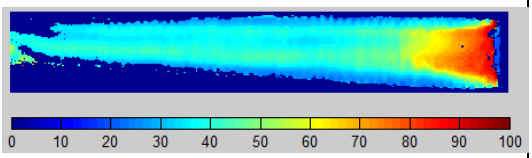

Table 7.4: Results for converging flow configuration - Re 3500 (T – narrow and Y – wide)

allowing it to accelerate in the narrow region from the entrance promoting turbulence by default. For the Reynolds numbers beyond 3500, the behavior is different in the

entire channel, since the entrance length effects are minimized as shown in Table 7.5, and Table 7.6. From this characteristic, it can be assumed that the flow is already turbulent when entering the channel. Entrance length effects in the case of higher Reynolds numbers, are minimized since there exists a faster rate of transverse

Reynolds Number and Case	**Heat transfer Coefficient, h, ($W/m^2 K$)**	**Pressure drop ratio**	**Heat transfer enhancement ratio**	**Heat transfer contour**
Re 8900 – Baseline	70.5 (T); 37.3 (Y)	1	1	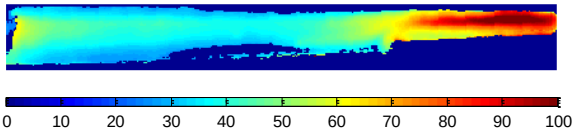
Re 8900 – Inline dimpled	119.7(T); 66.1(Y)	1.083	1.7(T); 1.77(Y)	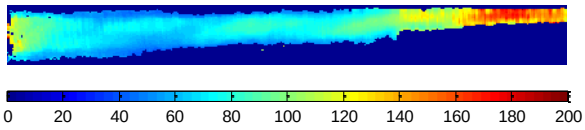
Re 8900 – Stagger dimpled	120.1(T); 56.2(Y)	1.167	1.7(T); 1.51(Y)	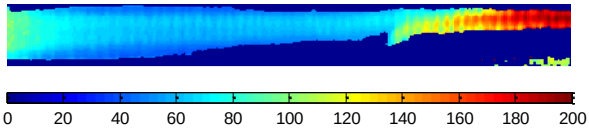

Table 7.5: Results for converging flow configuration - Re 8900 (T – narrow and Y – wide)

temperature distribution in the fully developed region. As the flow departs from the Reynolds number 3500, the rise in heat transfer coefficient can be seen with Reynolds

numbers 8900 and 18000, as shown in Table 7.5, and Table 7.6. The reason being the increase of convective heat fluxes. This effect is augmented even further, with the presence of dimples.

Reynolds Number and Case	**Heat transfer Coefficient, h, (W/m²K)**	**Pressure drop ratio**	**Heat transfer enhancement ratio**	**Heat transfer contour**
Re 18000 – Baseline	147.7 (T); 81.2 (Y)	1	1	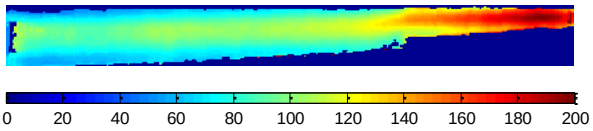
Re 18000 – Inline dimpled	161.7(T); 91.9(Y)	1.737	1.1(T); 1.13(Y)	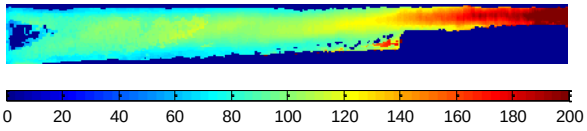
Re 18000 – Stagger dimpled	162.1(T); 92.3(Y)	1.789	1.1(T); 1.13(Y)	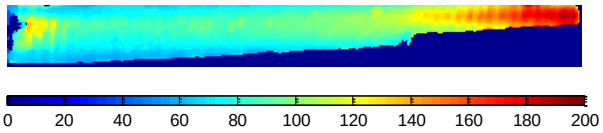

Table 7.6: Results for converging flow configuration - Re 18000 (T – narrow and Y – wide)

7.3 Correlation for the Dimpled Studies

Textbook definitions of correlation convey that it refers to a statistical relationship between two variables. It is a method used to quantify a deviation of two or more variables from independence. The study was carried out to determine correlations between Nusselt number (Nu) and Reynolds number (Re). A statistical correlation is measured by use of correlation coefficient which describes the degree of relationship between them. The results obtained from experimental testing will be used to develop the correlation. An accurate correlation of this nature will be of significant importance in the field of heat transfer, which could effectively enable dimpled enhancement feature to be extrapolated to wider range of problems.

A correlation study was performed on the sets of acquired data. All data points of Nusselt number from experimental data were plotted against the respective Reynolds number (based on the type of flow configuration). A regression analysis to fit a straight line through these data points may be represented as,

$$Nu = A\,Re^{b}$$

The coefficients A and b will in fact be a function of influencing parameters. In this study, it is the type of flow and the dimple configuration that decide these two coefficients. The above regression analysis is made to suit only the current stagger configuration of dimples that is under study.

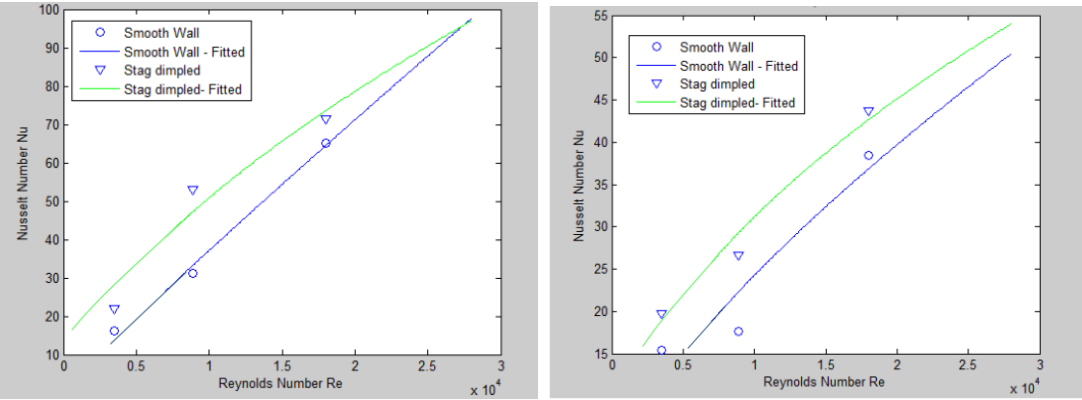

Figure 7.3: Correlation plots for the case of converging flow. (Left – narrow; right – wide)

Case	**Smooth Wall**		**Staggered dimpled**	
Constants	A	B	A	B
Narrow Area	6.467e-3	0.9397	0.15743	0.62739
Wide Area	3.4679e-2	0.7116	0.22962	0.5332

Table 7.7: Correlation constants for the case of converging flow.

MATLAB was used to compute the correlation with the sets of data attained by the experiments. Baseline and stagger dimple cases are compared to show the degree of enhancement attained for each case of Reynolds number. Figure 7.3 and Table 7.7 provide the trend and correlation constants for the case of stagger dimples with converging flow configuration. While, Figure 7.4 and Table 7.8 show the plots and correlation constants for baseline and stagger dimple cases in diverging flow configuration.

What seems evident from the data provided above is that Nusselt number shows a

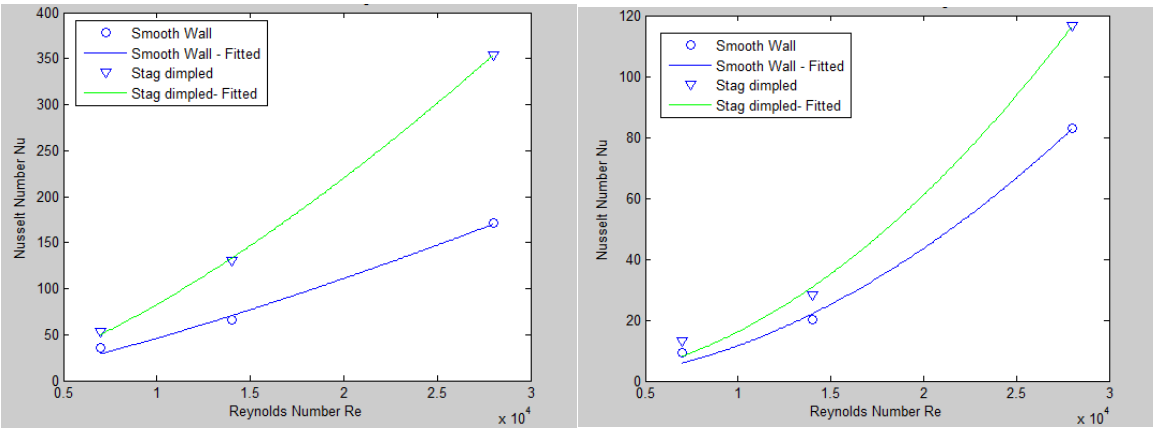

Figure 7.4: Correlation plots for the case of diverging flow. (Left – narrow; right – wide)

Case	**Smooth Wall**		**Staggered dimpled**	
Constants	A	B	A	B
Narrow Area	3.9e-4	1.2679	1.87e-4	1.4114
Wide Area	2.684e-7	1.9088	3.416e-7	1.9187

Table 7.8: Correlation constants for the case of diverging flow.

clear nonlinear dependency on the Reynolds number (Re), as expected. The Nusselt number (Nu) is calculated with the attained heat transfer coefficient using equation 6.8. The hydraulic diameter considered is averaged over the entire length for the wide and narrow section separately and used in the Nu calculation. Diverging flow configuration seems to have the best correlation fit with the equation chosen. In the case of converging flow, the curve fitted has some deviation from the data points due to uncertainties in the experiment. On taking log plots, the trend for the converging flow suggests that after a certain point, the increase in Nusselt number would be

reduced between Reynolds numbers. In the diverging flow case, the increase in Nusselt number would keep increasing for consecutive Reynolds numbers.

7.3.1 Comparison with Dittus-Boelter Equation

The Dittus-Boelter equation 6.7 is a common correlation used in the estimation of Nusselt number in a straight circular pipe, where forced convection is the only mode of heat transfer. This forms a good benchmark for comparison purposes. Figure 7.5 and Figure 7.6 show the comparison of experimental results with values from Dittus Boelter correlation in the case of smooth wall. It can be seen that for the case of converging flow, the trend follows that of Dittus-Boelter equation prediction for the specific Reynolds numbers. Dittus Boelter correlation has an associated uncertainty of ±15%. However, for both of the flow configurations, this correlation cannot be taken as an absolute yardstick. Mainly because, it is applicable only for a straight circular pipe and the channels employed in this study are of converging and diverging in nature with rectangular cross section. Meaning that the Dittus Boelter correlation does not take into account the acceleration and deceleration effects of the flow. These could be some or all of the reasons for the deviation of Nusselt number from the prediction. Hence, building a correlation for the dimpled channel becomes necessary.

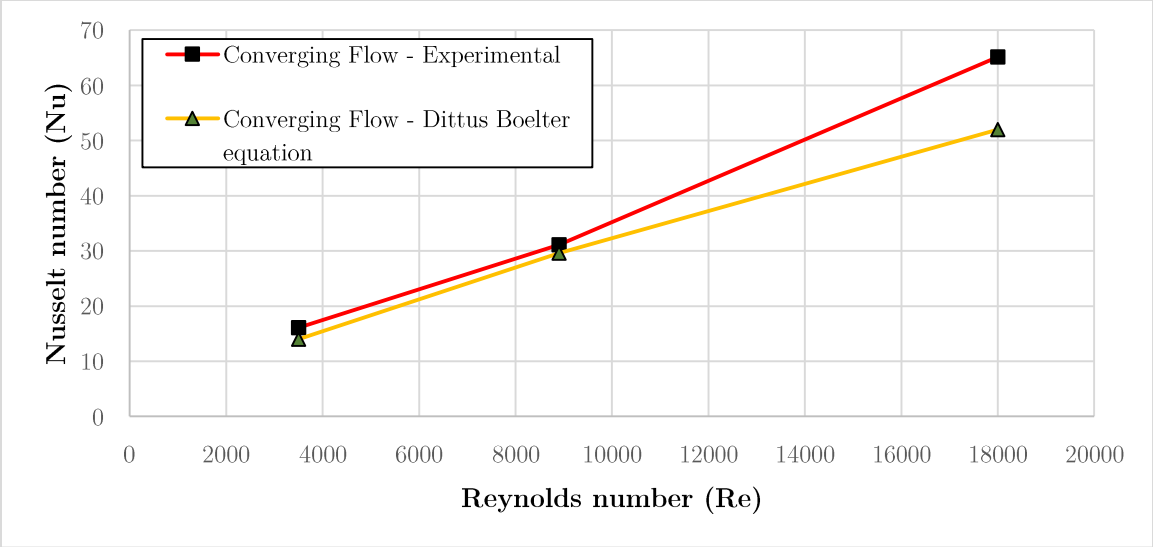

Figure 7.5: Comparison between Dittus Boelter equation and experimental results - converging flow.

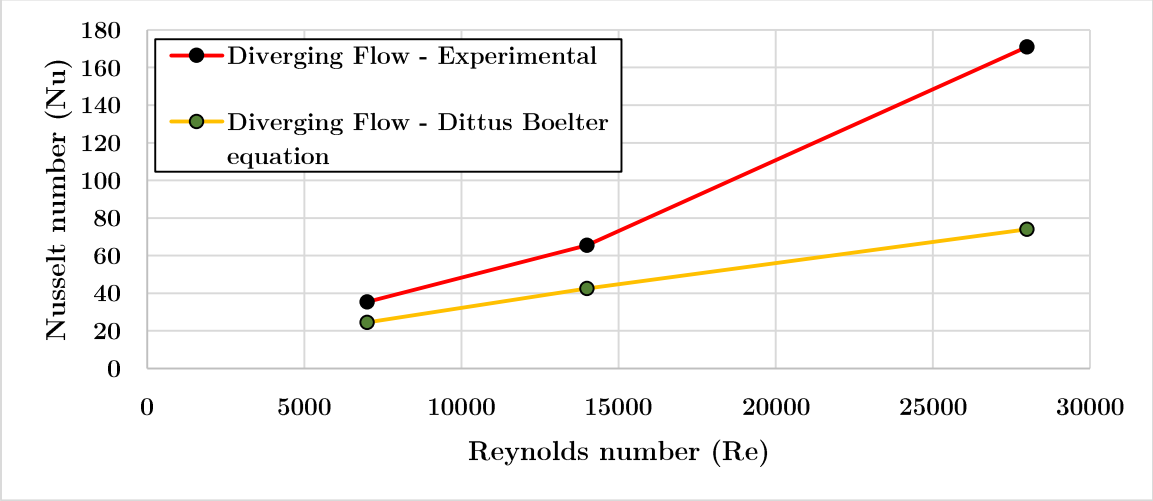

Figure 7.6: Comparison between Dittus Boelter equation and experimental results - diverging flow.

7.4 Strategic (Sequential and Random) Addition of Dimples on Test Section

The objective of this study was to explore where the placement of dimples would prove to be most effective in the channel for enhancement of heat transfer in diverging as well as the converging flow configurations. Several combinations of dimple placements are tested dimpled and smooth wall plates along the channel. Following are the results for diverging and converging flow combinations.

7.4.1 Diverging flow:

Cases	h(W/m^2 K)	Plots and results – wide region
	47.498	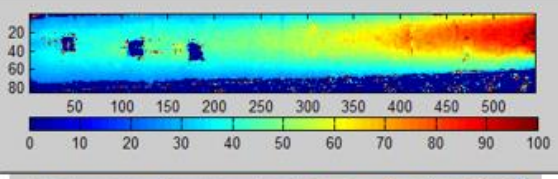
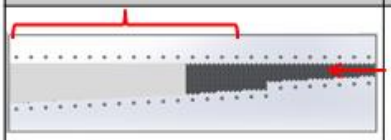	49.186	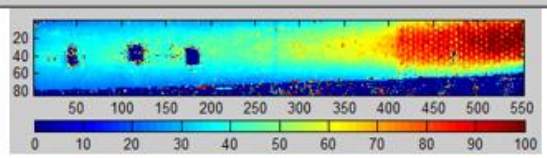
	53.318	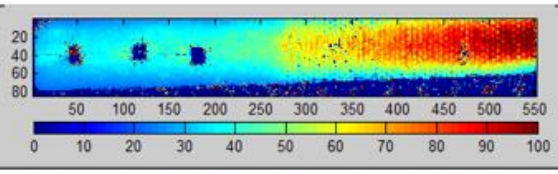
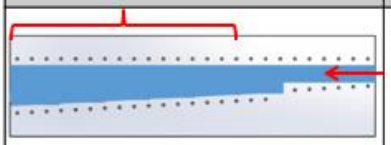	42.744	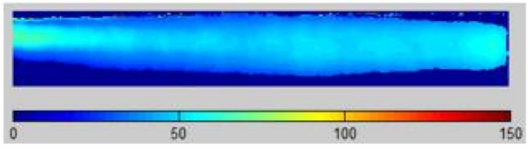
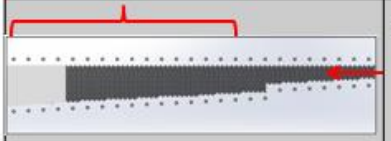	55.581	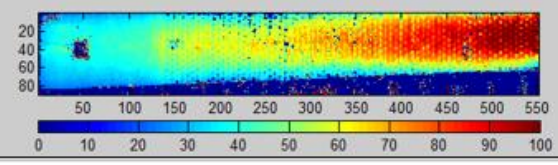

Table 7.9: Results for the diverging flow configuration on the increscent dimple test section.

In the case of diverging flow, only results on the Wide region are presented with the mixed configuration of dimples and smooth wall, since the narrow region was already explored with the previous test section. Only one Reynolds number of 14000 was explored in this configuration. Table 7.9 shows the results for diverging flow with incrementing dimpled area. For example, the first case shows the schematic of test section with only the narrow area dimpled, while the entire wide area remains smooth. In the next cases, along with the narrow region, 4 inches of Wide area is dimpled in a step wise fashion while the rest of the channel remains smooth. It can

Cases	h(W/m^2 K)	Plots and results – wide region
	53.946	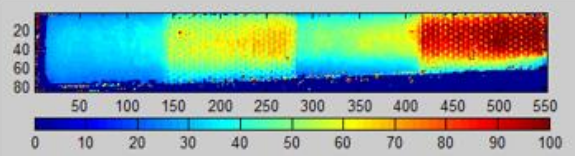
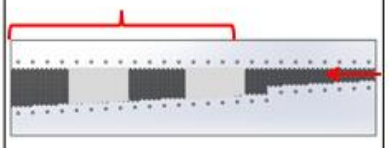	55.6723	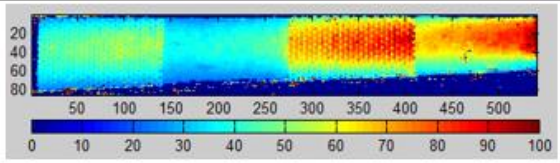
	56.749	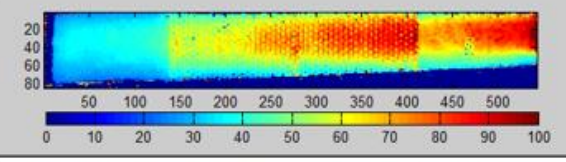
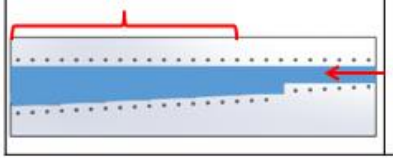	42.744	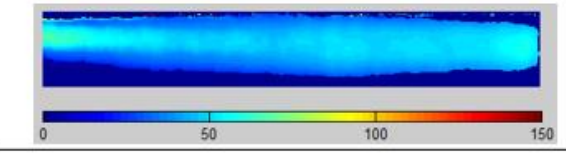

Table 7.10: Results for study of strategic placement of dimples - diverging flow.

be seen that as the surface area of dimples increase, the heat transfer coefficient increases proving the fact that dimples aid as a heat transfer enhancement feature

in diverging channels. A plot of baseline (blue region) is added in the table to show the augmentation achieved with the presence of dimples.

Table 7.10 provides results from the tests conducted with strategic configurations of dimples. Dark area represents the dimples in the schematic. It can be seen that patches of dimples are placed in different locations to find the critical region of heat transfer. With the results from Table 7.9, we can assume that as the surface area of dimples are made maximum, there would be maximum heat transfer. Results for such a case gives a heat transfer coefficient of about $56\,W/m^2K$. Third case on Table 7.10 provides the maximum heat transfer coefficient in comparison to the other cases. The maximum possible heat transfer is achieved with about half the surface area as the fully dimpled channel, proving that the location of dimples is a significant parameter in a diverging channel.

7.4.2 Converging Flow

Unlike the diverging flow, both narrow and wide sections are investigated in this flow configuration, since none of the cases overlap with the results from 7.2. Table 7.11 and Table 7.12 show results for converging flow configuration with combinations of dimple and smooth wall regions for a Reynolds number of 8900. The

Cases	h(W/m²K)	Plots and results – narrow region
	83.344	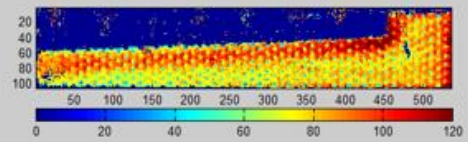
	90.598	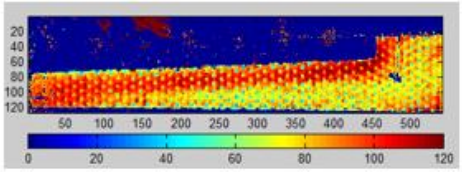
	99.165	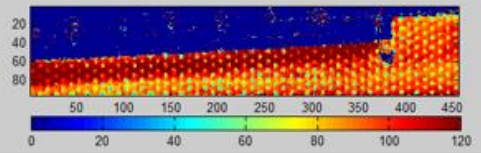
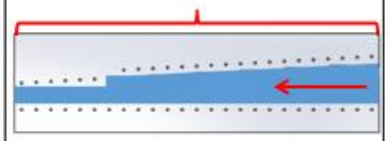	70.5(T) 37.3(Y)	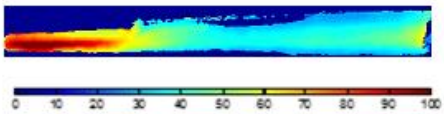
	105.611	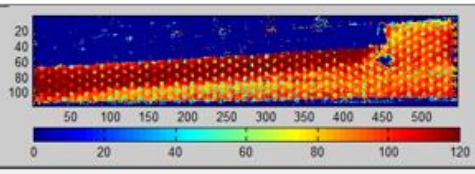

Table 7.11: Results for study of sequential configuration of dimples (Narrow Region) - Converging flow.

Cases	h(W/m² K)	Plots and results – narrow region
	102.841	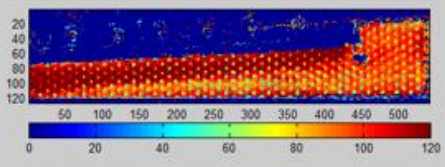
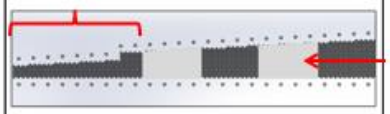	102.274	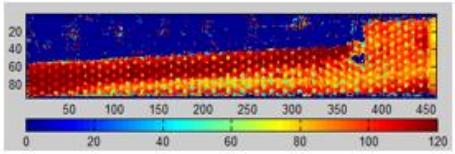
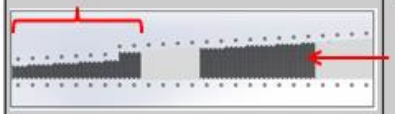	100.4092	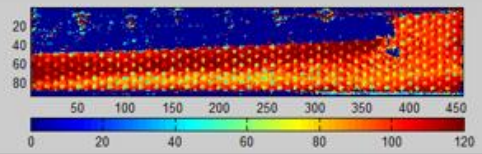

Table 7.12: Results for study of random placement of dimples (Narrow Region) - Converging flow.

narrow and wide regions are focused separately to understand the enhancement effects. The plots show that the presence of dimples in the wide region favor enhancement in heat transfer of narrow region to a significant extent. The shoulder

Cases	h(W/m² K)	Plots and results – wide region
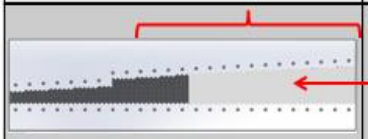	44.28	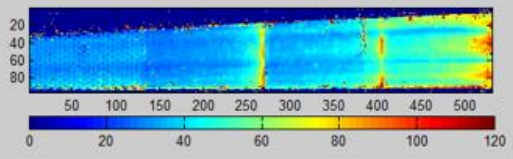
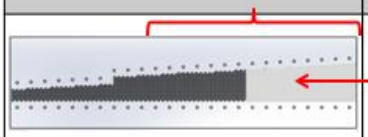	49.78	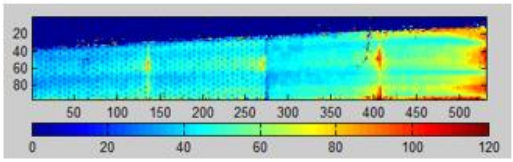
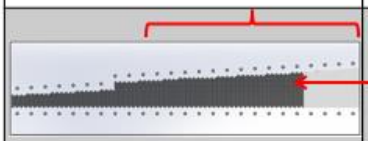	52.371	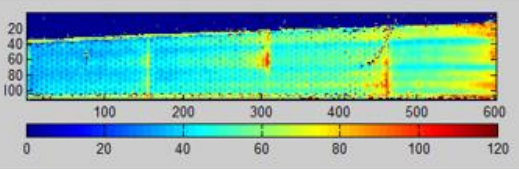

Table 7.13: Results for study of sequential configuration of dimples (Wide region) – Diverging flow.

Cases	h(W/m² K)	Plots and results – wide region
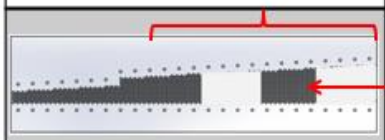	48.686	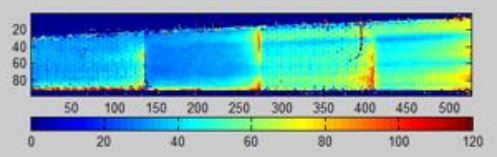
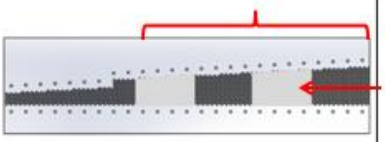	48.857	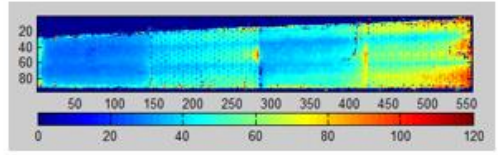
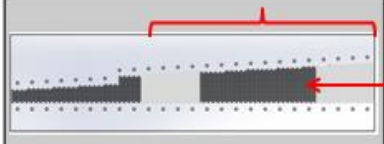	55.4427	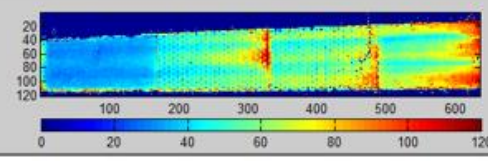

Table 7.14: Results for study of random configuration of dimples (Wide region) – Diverging flow.

region contributes in providing enhancement for the overall heat transfer in narrow region. The plots on Table 7.11 suggest that sequential addition of dimples directly increase the heat transfer augmentation.

The plots on Table 7.12 provide results for runs on the random addition of dimples across the channel. It can be seen that the presence of dimples in the wide region at any location translates into better heat transfer across the narrow section. The random addition of dimples in the wide section does not seem to affect the heat transfer in the narrow section as long as the dimples exist.

Results shown on Table 7.13 and Table 7.14 are for the wide section. Alike the narrow section, sequentially adding the dimples show an increase in heat transfer coefficient across the wide section of the channel. From the cases of random addition of dimples, the third configuration shows maximum heat transfer coefficient. On a channel that is entirely dimpled, a heat transfer coefficient of $56.2\ W/m^2K$ was seen. This value can be matched by just filling half the surface area with dimples.

8 Summary and Conclusions

This thesis focuses on examining heat transfer characteristics in channels with smooth-wall and dimpled configurations. The results indicate significant enhancement in the presence of dimples. Coolant channels ducts were created and tested in the stationary frame with diverging flow and converging flow cooling schemes. The intention is to replace at least a segment of an existing coolant channel with dimples (either Staggered or Inline). The models were created with clear acrylic material. Clear acrylic is necessary because of the transient liquid crystal technique used to measure the heat transfer coefficients. An airbrush is used to apply the liquid crystals and the black backing paint to the width walls of the channels.

Three different flow rates were examined on the test sections, values depending on the type of cooling scheme. For both cooling schemes, the enhancement in the narrow section is significant especially with the case of staggered dimples. On the overall, there is an enhancement of about 1.1 to 2.07 for narrow region and 1.08 to 1.7 for the wide region with the presence of dimples across the entire channel. The pressure drop is hardly observed at lower Reynolds numbers with the case of dimples in converging flow and diverging flow. On the whole, a pressure drop range of 1.16 to 1.7 was measured across the test channel. A correlation study was also made to confirm and quantify the behavior observed with experiments. The correlation trends

follow an exponential equation form, very similar to the present literature. Methods of sequential and random addition of dimples was examined to identify and understand the local significance of dimples across the channel. This configuration provides an understanding that location of enhancement can play an important role in heat transfer enhancement.

This study has provided a thorough insight about the capability of dimples. Dimples with larger diameters, dimples with non-circular geometry, pimples on dimples and many other configurations must be explored, since testing a complex geometry has been easier than ever with the capacity of the existing stationary test rig and also since any geometry (with dimensions of existing test-section) can be manufactured by 3D printing methods.

9 References

1. Afanasyev, V. N., Chudnovsky, Y. P., Leontiev, a. I., & Roganov, P. S. (1993). Turbulent flow friction and heat transfer characteristics for spherical cavities on a flat plate. *Experimental Thermal and Fluid Science*, *7*(1), 1–8. doi:10.1016/0894-1777(93)90075-T
2. Cooper, T. E., & Field, R. J. (2013). Liquid Crystal Thermography and Its Application to the Study of Convective Heat Transfer, (August 1975), 442–450.
3. Dhungel, A. (2007). FILM COOLING FROM A ROW OF HOLES SUPPLEMENTED WITH ANTI VORTEX HOLES, (August).
4. Gupta, S., Chaube, A., & Verma, P. (2012). Review on Heat Transfer Augmentation Techniques: Application in Gas Turbine Blade Internal Cooling., *5*(1), 57–62.
5. Isaev, S. a., Kornev, N. V., Leontiev, a. I., & Hassel, E. (2010). Influence of the Reynolds number and the spherical dimple depth on turbulent heat transfer and hydraulic loss in a narrow channel. *International Journal of Heat and Mass Transfer*, *53*(1-3), 178–197. doi:10.1016/j.ijheatmasstransfer.2009.09.042
6. Isaev, S. a., Leont'ev, a. I., Frolov, D. P., & Kharchenko, V. B. (1998). Identification of self-organizing structures by the numerical simulation of laminar three-dimensional flow around a crater on a plane by a flow of viscous incompressible fluid. *Technical Physics Letters*, *24*(3), 209–211. doi:10.1134/1.1262056
7. Isaev, S. A., Leontiev, A. I., Kudryavtsev, N. A., & Pyshnyi, I. A. (2003). The Effect of Rearrangement of the Vortex Structure on Heat Transfer under Conditions of Increasing Depth of a Spherical Dimple on the Wall of a Narrow Channel, *41*(2), 229–232.
8. Kornev, N., Turnow, J., Hassel, E., & Isaev, S. (n.d.). Fluid Mechanics and Heat Transfer in a Channel with Spherical and Oval Dimples, 231–237.
9. Kovalenko, G. V., Terekhov, V. I., & Khalatov, A. A. (2010). FLOW REGIMES IN A SINGLE DIMPLE ON THE CHANNEL SURFACE. *Journal of Applied Mechanics and Technical Physics*, *51*(6), 839–848.
10. Lamont, J. A., Roy, C. J., & Stern, C. H. (2012). Heat Transfer in Stationary and Rotating Coolant Channels Using a Transient Liquid Crystal Technique Heat Transfer in Stationary and Rotating Coolant Channels Using a Transient Liquid Crystal Technique.

11. Lienhart, H., Breuer, M., & Köksoy, C. (2008). Drag reduction by dimples? – A complementary experimental/numerical investigation. *International Journal of Heat and Fluid Flow*, *29*(3), 783–791. doi:10.1016/j.ijheatfluidflow.2008.02.001
12. Ligrani, P. (2013). Heat Transfer Augmentation Technologies for Internal Cooling, *2013*.
13. Ligrani, P. M., Harrison, J. L., Mahmmod, G. I., & Hill, M. L. (2001). Flow structure due to dimple depressions on a channel surface. *Physics of Fluids*, *13*(11), 3442. doi:10.1063/1.1404139
14. Mahmood, G. ., & Ligrani, P. . (2002). Heat transfer in a dimpled channel: combined influences of aspect ratio, temperature ratio, Reynolds number, and flow structure. *International Journal of Heat and Mass Transfer*, *45*(10), 2011–2020. doi:10.1016/S0017-9310(01)00314-3
15. Mcguire, E. C., & Abdelmessih, A. N. (2011). LITERATURE REVIEW OF SINGLE PHASE INTERNAL FLOW HEAT TRANSFER CORRELATIONS IN STRAIGHT CIRCULAR CONDUITS, 1–11.
16. Silva, C., Marotta, E., & Fletcher, L. (2007a). Flow Structure and Enhanced Heat Transfer in Channel Flow With Dimpled Surfaces: Application to Heat Sinks in Microelectronic Cooling. *Journal of Electronic Packaging*, *129*(2), 157. doi:10.1115/1.2721087
17. Silva, C., Marotta, E., & Fletcher, L. (2007b). Flow Structure and Enhanced Heat Transfer in Channel Flow With Dimpled Surfaces: Application to Heat Sinks in Microelectronic Cooling. *Journal of Electronic Packaging*, *129*(2), 157. doi:10.1115/1.2721087
18. Slabaugh, C. D., Tran, L. V., & Kapat, J. S. (2011). Heat Transfer in a Rectangular Channel with Dimples Applied to One Wall. *Journal of Propulsion and Power*, *27*(6), 1303–1314. doi:10.2514/1.B34190
19. Snedeker, R. S., & Donaldson, C. D. (1966). Observation of a Bistable Flow in a Hemispherical Cavity. *AIAA*, *3903*(APRIL), 735–737.
20. Souza Mendes, P. R. (1991). The naphthalene sublimation technique. *Experimental Thermal and Fluid Science*, *4*(5), 510–523. doi:10.1016/0894-1777(91)90031-L
21. Stone, K. M. (1996). Review of Literature on Heat Transfer Enhancement in Compact Heat Exchangers Amana Refrigeration , Inc . Carrier Corporation Caterpillar , Inc . Dayton Thermal Products Delphi Harrison Thermal Systems Eaton Corporation Ford Motor Company Frigidaire Compan, *61801*(August).

22. Terekhov, V. I., Barsanov, V. L., Kalinina, S. V, & Mshvidobadze, Y. M. (2006). AND HEAT TRANSFER UNDER A JET FLOW PAST A SPHERICAL-CAVITY OBSTACLE, *79*(4), 29–37.
23. Turnow, J., Zhdanov, V., Hassel, E., & Kornev, N. (2003). Flow structures and heat transfer on dimpled surfaces, 1–6.
24. Won, Y., & Ligranr, P. M. (2007). Flow characteristics along and above dimpled surfaces with three different dimple depths within a channel, *21*, 1901–1909.
25. Xie, G., Sundén, B., & Zhang, W. (2011). Comparisons of Pins/Dimples/Protrusions Cooling Concepts for a Turbine Blade Tip-Wall at High Reynolds Numbers. *Journal of Heat Transfer*, *133*(6), 061902. doi:10.1115/1.4003558